Appendix A: The element by element analysis

All the elements which contribute to the spectrum of HD 175640 are individually considered here. Table A.1, Table A.2, and Table A.3 list respectively the lines of the light elements, of the iron group elements and of the elements with atomic number Z$\geq$30 which were analyzed for abundance purposes. In all three tables the lines of each element are arranged in increasing wavelength order. Multiplet numbers are mostly taken from Moore (1972), except for He I. In this case multiplet numbers from NIST and from Wiese et al. (1966) (the ones in parenthesis) are given. For each line, the log gf value, its reference, and the lower excitation potential are listed. In Table A.1 the Stark damping constant $\log(\gamma_S/N_e)$ for T=20000 K and its reference are added. There are no damping constants for He I in Table A.1 because they were obtained by interpolating for temperature and, for a few lines, also for electron and ion density, in tables of Stark broadening parameters or Stark profiles (Sect. 4), whose reference can be found in col. 7. In Table A.3, the excitation potential of the upper level is added. In all the tables the last three columns show the measured equivalent width, the corresponding abundance, and the remarks, if any needed. When no equivalent width is given the abundance was derived from the comparison of observed and computed profiles. This kind of determination was mostly performed when different transitions belonging to the same multiplet are observed as a single profile. The average abundance and its standard deviation (when more lines were measured) are given at the top of the subtable relative to the given ion.

Helium (2)-He I: By varying the He abundance in steps of 0.01 dex we obtained $\log(N(He)/N_{\rm tot})=-1.73$ (i.e. [−0.62]) from the comparison of the computed and observed profiles of the lines listed in Table A.1. All the weak lines are fully consistent with the adopted abundance, while some differences between observations and computations occur for the strongest lines. Fig. A.1 shows that the blue wing of λ 4026 Å is not well reproduced, while the computed cores of $\lambda\lambda$ 4471 and 6678 Å are slightly too strong. We did not find any trace of the ^{3}He isotope for the line at 6678 Å, so that we assumed that the He isotopic ratio is the terrestrial one.

The weakness of all the He I lines observed in HD 175640 may justify the LTE assumption.

Beryllium (4)-Be II: The only unblended line observed in the spectrum is the Be II resonance line at 3130.420 Å, mult. 1. The abundance $\log(N(Be)/N_{\rm tot})=-10.64$ derived from the equivalent width is solar. Sadakane et al. (1985) found $\log(N(Be)/N(H))<-9.7$ from IUE spectra. The other Be II line of mult. 1 at 3131.065 Å is predicted weak for the above abundance and is heavy blended with Mn II. A weak unidentified absorption at 5270.3 Å can hardly be due to Be II 5270.28 Å mult. 3 as the other, stronger line of the same multiplet at 5270.815 Å is not observed.

The log gf values of the Kurucz line list, which were taken from Biémont et al. (1977), were used for the lines examined here. They do not differ by more than 0.005 dex from those available in the NIST database.

Boron (5)-Not observed: There are no observed absorptions at the position of B II 3451.287 Å, mult. 1. An absorption at 3451.32 Å identified as Fe II 3451.318 Å is much stronger than predicted both when log $gf=-1.519$ from the Kurucz database and log $gf=-1.651$ from Raassen & Uylings (1998) are used. We could speculate that boron contributes to the observed absorption, provided that its wavelength is 3451.320 Å and that it is highly overabundant. However, Sadakane et al. (1985) derived from IUE spectra a boron underabundance of the order of [−1.4]. Therefore we assume that no boron lines are observable in our spectra.

Carbon (6)-C I,C II: The most striking characteristic of carbon is the presence of the two strong emission lines of C I mult. 10 at 8335.148 Å and and C I mult. 9 at 9405.730 Å. They are shown in Fig. A.2, where the observed spectrum, the computed spectrum and the telluric spectrum are superimposed.

There is no doubt that the carbon abundance is subsolar, but it is difficult to fix its exact value owing to the position of the strongest C I and C II lines in the red part of the spectrum where they are either embedded in strong telluric absorptions or heavily blended with them. Examples are C I mult. 3 at 9061.431 Å, 7231.33 Å and 7236.42 Å and C I mult. 2 at 9620.777 Å and 9658.430 Å. In addition, the spectrum is of bad quality in the 9074-9098 Å region, just where three C I lines of mult. 3 ($\lambda\lambda$ 9078.288, 9088.513 and 9094.830 Å) could have been measured.

The few C I and C II lines that have measurable equivalent widths are listed in Table A.1. We remark that C II mult. 4 at 3918.968 Å seems to blueshifted relatively to the wavelength taken from Wiese et al. (1996). If the shift is not real it could be blended with an unknown component. The average abundance from C I is -4.11 ± 0.23 dex, that from C II is -4.05 ± 0.16 dex, while the average abundance from all C I and C II lines is -4.08 ± 0.20 dex. After comparison of the synthetic spectrum with the observed spectrum we assumed $\log(N(C)/N_{\rm tot})=-4.00$.

According to Hempel & Holweger (2003) no NLTE corrections are needed for the carbon lines examined in HD 175640 because no negligible NLTE effects are predicted in late B-type stars for lines with equivalent widths larger than 100 mÅ .

Nitrogen (7)-Not observed: There are no nitrogen lines observed in the spectrum. The computed N I lines of mult. 1 at 8680-8728 Å disappear for $\log(N(N)/N_{\rm tot})=-5.78$. We

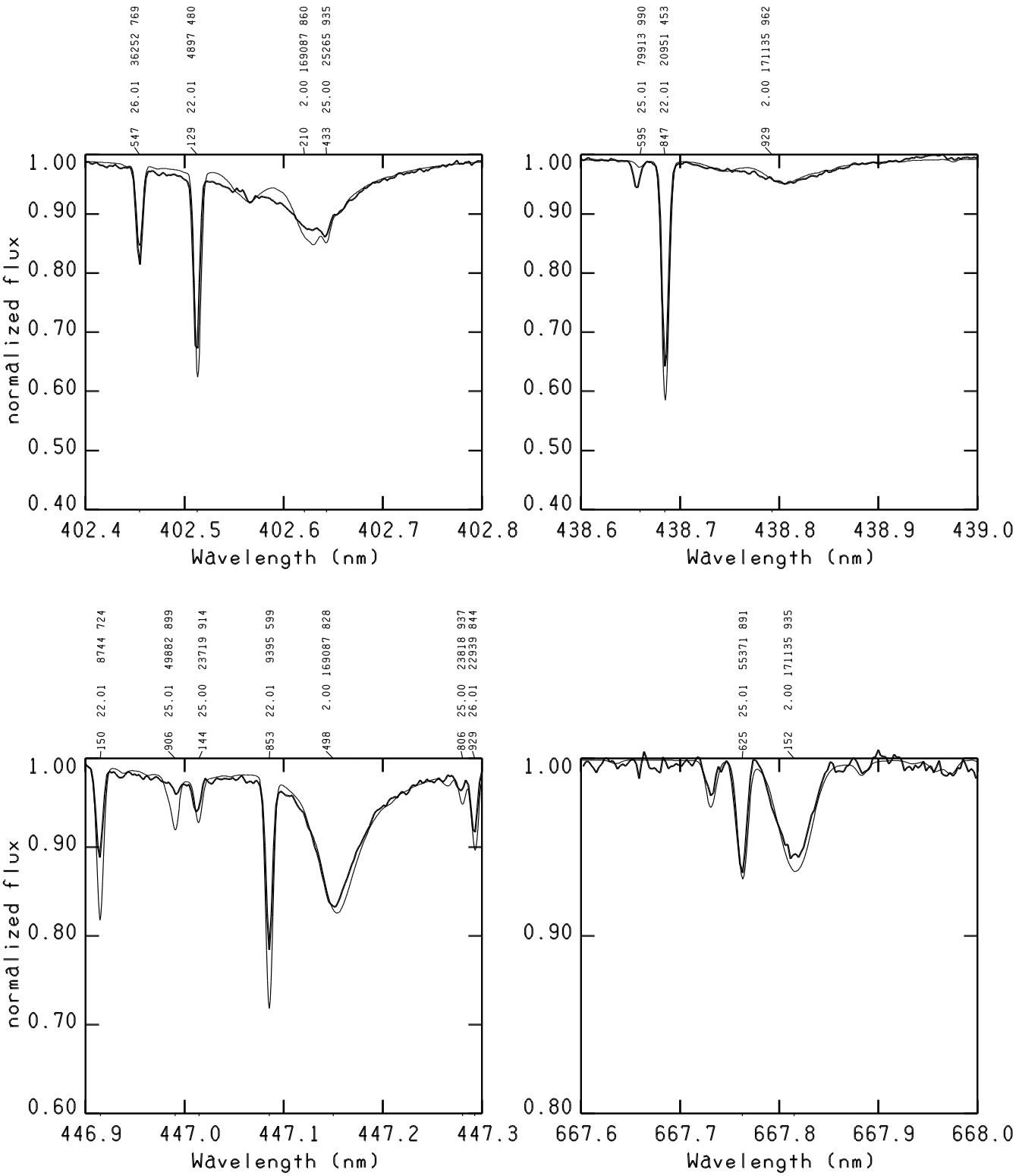

Fig. A.1. Comparison of observed (thick line) and computed (thin line) profiles of He I 402.6, 438.7, 447.1 and 667.8 nm. The meaning of the line identification labels like 547 26.01 36252 769 is: 547, last 3 digits of wavelength in nm (402.4547); 26.01, element (26) and charge (01), i.e. Fe II; 36252, lower energy level in cm^{-1}; 769, per mil residual flux of isolated line before rotation

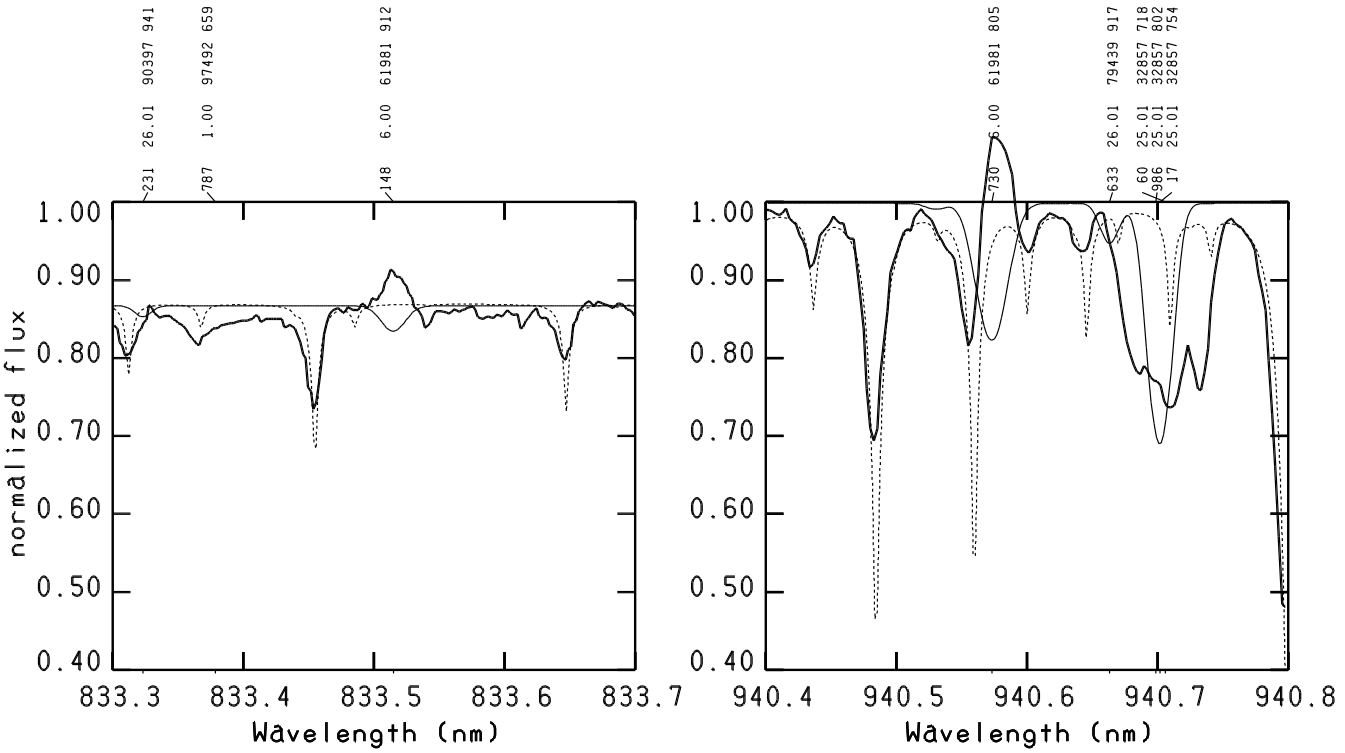

Fig. A.2. Observed emissions at the position of C I 833.5148 nm and C I 940.5730 nm. Observed spectrum (thick line), stellar synthetic spectrum (thin line), and telluric synthetic spectrum (dotted line) are superimposed. The meaning of the identification labels is the same as that given in the caption of Fig. A.1

adopted this value as upper limit for the nitrogen abundance. It corresponds to an underabundance of [−1.66].

Oxygen (8)-O I,O II: We identified a large number of O I lines, and two O II lines of mult. 1 (4641.82 Å and 4649.14 Å) that were so weak that no measurements of their equivalent widths were performed. All the O I lines analyzed in the spectrum are listed in Table A.1.

Owing to the triplet and quintet nature of most of the transitions, the oxygen abundance was estimated both from the profiles and from the equivalent widths. The adopted final value $\log(N(O)/N_{tot})=-3.18\pm0.11$ is the average abundance derived only from the equivalent widths, provided that the lines of multiplets 1, 4 and 8 and all the lines with Stark broadening parameter not available from the literature are excluded from the mean. In fact, lines computed with the approximate Stark profiles of the SYNTHE code are too strong, as are the lines of mult. 14 at 4967-4968 Å. Furthermore, the comparison of the LTE computed spectrum with the observed spectrum has shown the inadequacy of the LTE models for reproducing the infrared strong O I lines, in particular those of mult. 1, 4 and 8 at 7773.4 Å, 8446.5 Å and 9263.9 Å, respectively. Numerous papers deal with the NLTE corrections for these lines in B-type stars. The most recent one is Hempel & Holweger (2003). We point out that the observed profiles of these lines cannot be reproduced in LTE even when the LTE overabundance derived from the measured equivalent widths is adopted. Fig. A.3 compares the observed profiles of the O I triplet at 7773.4 Å with profiles computed with two different abundances, −3.18 dex and −2.10 dex. The first abundance is the one we adopted for oxygen in HD 175640 while the second abundance is the one we derived from the equivalent widths of the lines of O I triplet mult. 1. In the first case the computed cores are much weaker than the observed ones, in the second case the increased abundance increases not only the cores but also the wings, so that the profiles become broader and broader and will never agree with the observed ones.

The −3.18 dex oxygen abundance is only +0.3 dex larger than the solar one (Grevesse & Sauval 1998). However, a detailed NLTE analysis of O I lines is required before drawing any conclusion on the oxygen abundance in HD 175640.

Neon (10)-Ne I: Only very weak lines of Ne I were identified. The equivalent width of Ne I at 7032.4131 Å, mult. 1 gives $\log(N(Ne)/N_{tot})=-4.35$. All the weak observed lines agree with the lines predicted by this abundance. An example is Ne I at 6506.528 Å. Neon is therefore underabundant by about 0.4 dex with respect to the solar abundance. Dworetsky & Buday (2000) assign an upper limit $\log(N(Ne)/N(H))\leq-4.9$ to the neon abundance obtained from an NLTE analysis.

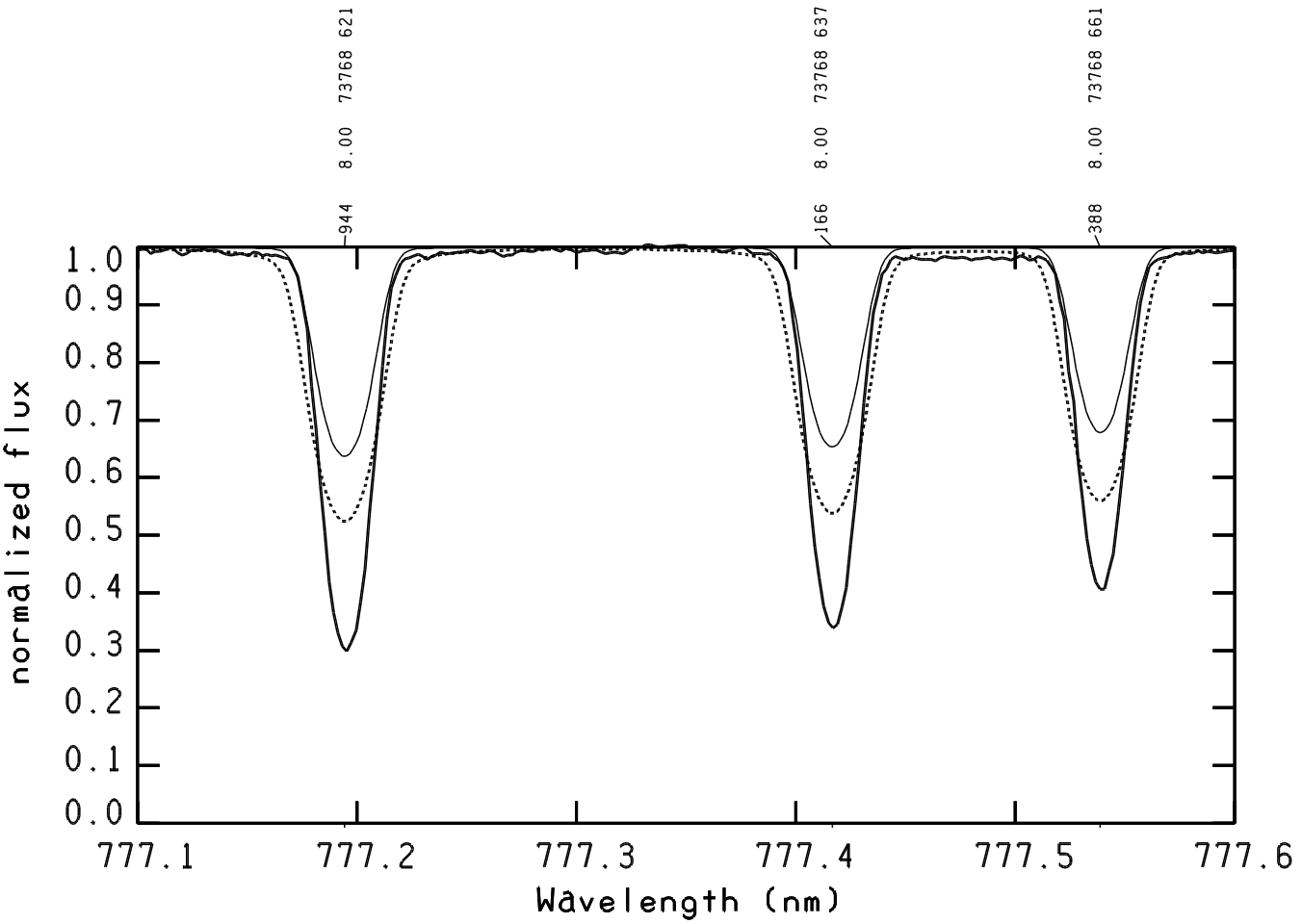

Fig. A.3. Synthetic LTE profiles of O I triplet mult. 1 at 777.2-777.5 nm computed with two different oxygen abundances, −3.18 dex (thin line) and −2.10 dex (dotted line), are compared with the observed profiles (thick line). The first abundance is the average abundance from selected equivalent widths (see text) the second abundance is that derived from the equivalent widths of the O I triplet mult. 1 lines. Increasing the O I abundance does not reduce the disgreement between the observed and computed profiles The meaning of the identification labels is the same as that given in the caption of Fig. A.1

Sodium (11)-Na I: All the Na I lines observed in the spectrum (Table A.1) are either blended with telluric lines or are affected by a red component of interstellar or circumstellar origin, as are the lines of mult. 1 at 5889.95 Å and 5895.92 Å. For this reason, the abundance $\log(N(Na)/N_{tot})=-5.47$, corresponding to an overabundance of +0.2 dex, is only a rough estimate.

Magnesium (12)-Mg I,Mg II: Several Mg I and Mg II lines can be observed in the spectrum, but only a few of them are unblended. Almost all the lines in the red part of the spectrum are affected by telluric absorptions, as for instance the two strong lines of Mg II mult. 1 at 9218.25 Å and 9244.26 Å, so that they can not be used for any abundance determination. Furthermore, there are some lines for which the Stark broadening parameters are lacking, like Mg II at 5401.52 Å and at 5401.56 Å, so that their computed profiles are very different from the observed ones.

The average abundance from Mg I lines with measurable equivalent widths is −4.64±0.06 dex, that from Mg II is −4.71±0.07 dex, while the average abundance from all the Mg I and Mg II lines is $\log(N(Mg)/N_{tot})=-4.69\pm0.07$, corresponding to an underabundance of [−0.23]. The average Mg abundance gives an excellent agreement between the observed and computed wings of the Mg II lines at 4481 Å, but the computed cores are less deep than the observed ones.

Smith (1993) derived $\log(N(Mg)/N(H))=-5.00\pm0.18$ from IUE spectra.

Aluminium (13)-Not observed: There are no aluminium lines observed in the spectrum, except for a feature at 4663.05 Å, which could be identified as Al II mult. 2 at 4663.046 Å. However, the abundance $\log(N(Al)/N_{tot})=-6.75$ from the measured equivalent width 4.51 mA is too high when used to predict all the other unobserved Al I and Al II lines. We therefore assumed that this line is due

to some other unidentified element. The computed lines of Al I mult. 1 at 3944.009 Å and 3961.523 Å disappear for the abundance −7.50 dex, which corresponds to an underabundance [−1.93]. We adopted this value as upper limit for the aluminium abundance.

From IUE spectra Smith (1993) derived log(N(Al)/N(H))=−7.02±0.31.

Silicon (14)-Si II,Si III: Numerous Si II lines and two weak Si III lines of mult. 2 at 4552.6 Å and 4567.8 Å were observed in the spectrum. The intense Si I line of mult. 3 at 3905.52 Å is heavily blended with a strong unidentified component, which is very probably a too weak predicted Mn II line at 3905.452 Å.

It was not easy to fix the Si abundance from the Si II lines on the basis of the Kurucz line lists only. In fact, they include all the Si II lines of the Moore (1965) multiplet tables, but missing Stark broadening parameters for some lines and the use of guessed oscillator strengths in several cases produced discordant abundances from the different lines. We implemented the silicon atomic data in the Kurucz line lists by replacing numerous guessed log gfs with those we derived from the multiplet oscillator strengths available in Lanz & Artru (1985) (LA) and by adding the radiative and Stark broadening parameters from Lanz, Dimitrijević & Artru (1988) for a few lines.

We compared a few Si II oscillator strengths of the Kurucz line lists taken from Kurucz & Peytremann (1975)(KP) with log gfs from LA. They agree for almost all the lines. However, the KP log gfs of a few lines not studied by LA produced profiles much stronger than the observed ones. These lines are Si II mult. 20 at 3997.926 Å and Si II at 4002.592 Å, 4028.465 Å and 4035.278 Å due to the $3p^2\,{}^2P-3d'\,{}^2D$ transition. The KP log gfs of the last three lines, −0.610, −0.360 and −1.300 were replaced by −2.75, −3.10 and −2.60 derived from the comparison of observed and computed profiles when the Si II average abundance −4.72 dex from Table A.1 is adopted. Also the guessed log gfs of the Si II lines at 3991.780 Å and 4016.188 Å produce profiles which do not fit the observed spectrum.

We measured the equivalent widths of the Si II and Si III lines listed in Table A.1. The average abundances are −4.72±0.08 dex and −4.58±0.04 dex, respectively. The average abundance from all Si II and Si III lines is −4.71±0.09 dex, which was adopted as final silicon abundance.

The LTE synthetic spectrum does not correctly predict the strong Si II lines of mult. 2 at 6347.11 Å and 6371.37 Å. The behaviour is analogous to that we showed in Fig. A.3 for the O I lines of mult. 1. The cores of the observed profiles are stronger than those computed for the average abundance −4.71 dex, while the observed wings are narrower than the computed ones. An increase of the abundance increases both the cores and the wings of the computed profiles, so that their shape is always different from that observed in the spectrum.

From IUE spectra Smith (1993) derived log(N(Si)/N(H))=−4.60±0.10.

Phosphorus (15)-P II: Only weak P II lines can be observed in the spectrum. We did not any change in the Kurucz line lists, except for the log gf of the lines at 3505.995 Å, 3786.581 Å and 6301.933 Å which yield computed lines which are not observed. In spite of Hibbert (1988) being the source quoted by Kurucz for these lines, a check of the log gfs derived from the transition probabilities A_l listed by Hibbert (1988) has shown that they are different from those of the Kurucz line lists. We derived −4.540, −2.719 and −2.455, respectively. The measured equivalent widths of the lines listed in Table A.1 give $\log(N(P)/N_{tot})=-6.28\pm0.08$, corresponding to an overabundance of [+0.3].

Sulfur (16)-S I,S II: Several weak S II lines can be observed in the spectrum. The average abundance from the measured equivalent widths (Table A.1) is −5.12±0.3 dex, corresponding to the underabundance [−0.41].

For this abundance, the lines of S I mult. 1 at 9212.863 Å and 9237.538 Å are predicted to be much weaker than what is observed. Possibly, NLTE computations could explain the discrepancy. We did not use them for the abundance determination.

Calcium (20)-Ca I,Ca II: There is a large scatter in the abundances derived from Ca I and Ca II and also from the different Ca II lines.

Only Ca I mult. 2 at 4226.728 Å is observed. The abundance from the equivalent width is $\log(N(Ca)/N_{tot})=-5.26$.

Most of the relevant Ca II lines lie on the wings of hydrogen profiles, except Ca II mult. 4 at 3158.8 Å, 3179.3 Å and 3181.2 Å. The average abundance from the equivalent widths of the three lines is $\log(N(Ca)/N_{tot})=-5.83\pm0.06$. Abundances from other lines were derived by comparing observed and computed profiles. Both lines of Ca II mult. 1 at 3933.663 Å (K-line) and 3968.469 Å (H-line) are affected by a red component of unknown origin (Fig. A.4). While a small bump is detectable on the red side of the K-line core, a component is well detectable on the red wing of the H-line. If the red components are neglected, the abundance from the H and K profiles is $\log(N(Ca)/N_{tot})=-5.54$, in agreement with the abundances from other Ca II lines observed in the 3700-6000 Å region, which range from −5.54 to −5.64 dex.

There are only two lines of the infrared Ca II triplet that can be observed in the spectrum. They are λλ 8498.023 Å and 8662.141 Å; the third line at 8542.091 Å is lost in the gap between the UVES èchelle orders. The two Ca II lines are redshifted by 0.2 Å from the expected position of the laboratory wavelength. This shift was explained by Castelli & Hubrig (2004) as due to an anomalous Ca isotopic mixture, in which the heaviest stable isotope ^{48}Ca is more abundant than the isotope ^{40}Ca, which

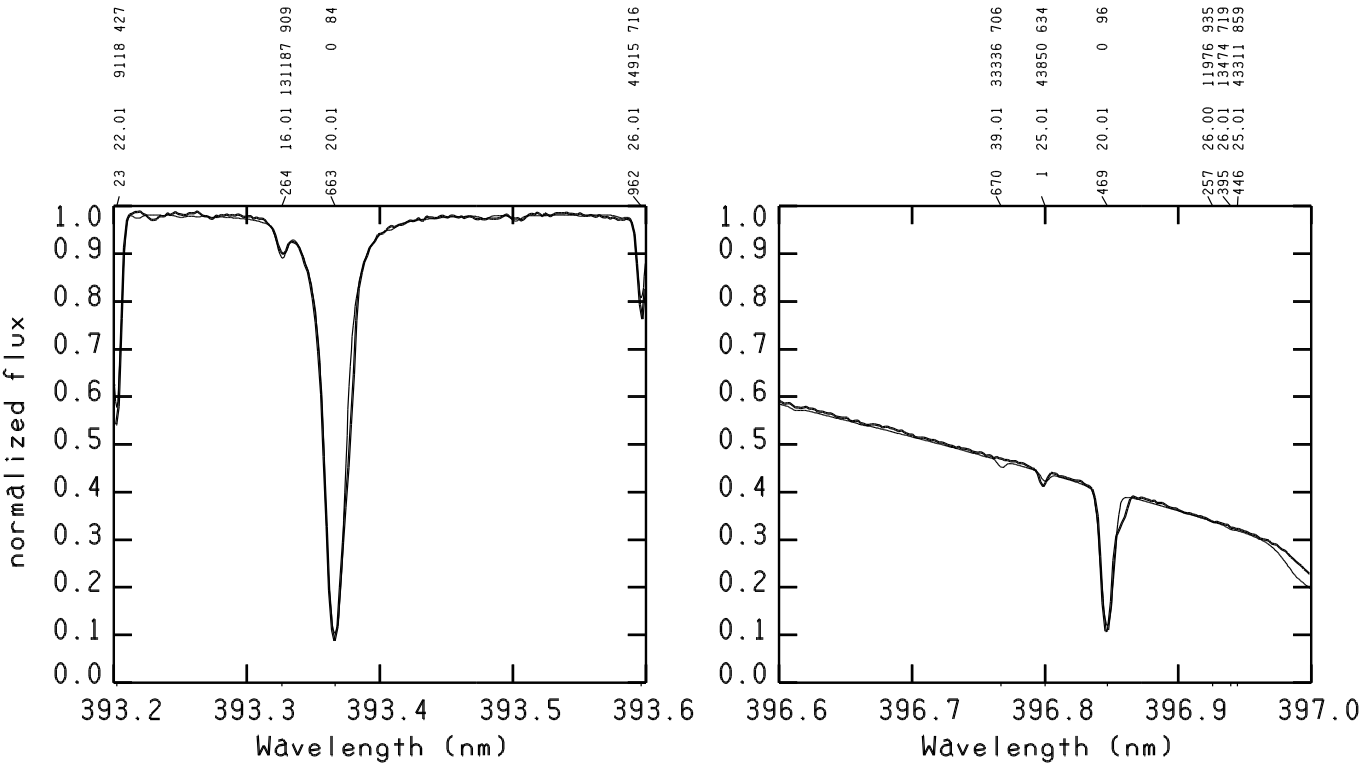

Fig. A.4. Comparison of the observed Ca II K and H profiles (thick line) with the computed ones (thin line). A bump can be observed on the red side of Ca II K while an unidentified red component is well detectable on the red wing of Ca II H. The meaning of the identification labels is the same as that given in the caption of Fig. A.1

is instead the predominant one in the terrestrial mixture. While the abundance from the first profile is −5.54 dex in agreement with the determinations from most Ca II lines, the abundance from the second profile is more than 0.3 dex larger, indicating possible NLTE effects.

Also the Ca II doublet at 8912.07 Å and 8927.36 Å is observable, but the lines predicted by the abundance of −5.54 dex are much stronger than what is observed. We did not use them for the average abundance determination owing to the unknown accuracy of their log gfs taken from Kurucz & Peytremann (1975). No other log gf sources for these lines were found. Both profiles are redshifted by about 0.03 Å, but this value is close to the uncertainties in the wavelength scale.

The line at 8248.796 Å, Ca II mult. 13, is a weak observed feature reproduced by an abundance of −6.40 dex.

We adopted as final abundance for computing the synthetic spectrum $\log(N(Ca)/N_{tot})=-5.54$.

Scandium (21)-Sc II: The abundance from the near-ultraviolet Sc II lines is solar and is 0.3 dex higher than that from the visual lines. We adopted as final value the average abundance from all the Sc II lines, $\log(N(Sc)/N_{tot})=-9.08\pm0.15$ dex.

Titanium (22)-Ti II: We identified numerous Ti II lines. All the lines with high excitation potential ($\chi_{low} \geq\sim$ 62000 cm^{-1}, i.e. 7.7 eV) and large transition probabilities (log $gf > -1.00$) are in emission. They can be observed starting from Ti II at 5846.579 Å. All the identified Ti II emission lines are listed in Table A.4. The columns R_c(obs) and R_c(calc) give the flux normalised to the continuum at the center of the line in the observed and synthetic spectra, respectively. R_c(obs) is a measure of the intensity of the observed emission. We assumed that some lines listed in Table A.4, although observed as absorptions, are affected by an emission reducing their intensity. They are all the lines with $R_c(obs) \leq 1.0$. Owing to the uncertainties in the position of the continuum and in the log gf data, the only unquestionable emissions are those with $R_c(obs)\geq1.01$. Fig. A.5 shows the Ti II emission at 6029.27 Å.

We adopted wavelengths and experimental log gfs from Pickering et al. (2002) for most of the Ti II lines with $\lambda<5500$ Å instead of the data from the Kurucz files, although several of them are from the Martin, Fuhr & Wiese (1988) critical compilation. We found that the Pickering et al. (2002) data improve the agreement between the observed and computed spectra considerably.

Abundances from equivalent widths are given in Table A.2. The average abundance is −5.67±0.11 dex, so that Ti is overabundant by 1.35±0.11 dex. However, there is a small difference of 0.13 dex between the average abundance from lines shortward and longward of the Balmer discontinuity. The values are −5.59±0.09 dex and −5.72±0.08 dex, respectively.

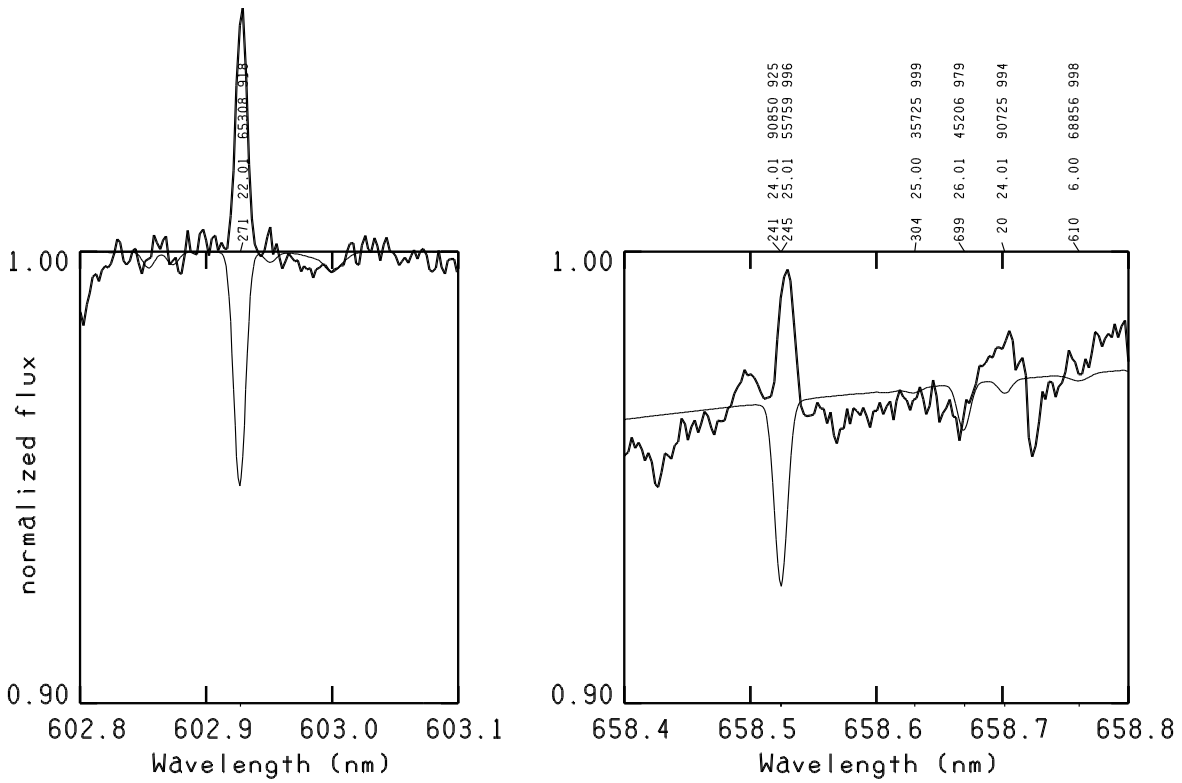

Fig. A.5. Observed emission lines at the position of Ti II 602.9271 nm (left panel,thick line) and of Cr II 658.5241 nm and Cr II 658.7020 nm (right panel, thick line). The thin line is the synthetic spectrum. The meaning of the identification labels is the same as that given in the caption of Fig. A.1

Vanadium (23)-Not observed: No lines of vanadium were observed in the spectrum. We fixed an upper limit of -9.04 dex for the vanadium abundance from V II mult. 1 at 3100 Å. It corresponds to an underabundance [V/H]$=-1.0$,

Chromium (24)-Cr I,Cr II: We identified several Cr I and numerous Cr II lines. All the Cr II lines with high excitation potential (χ_{low} larger than 89000 cm^{-1}, i.e. 11 eV) and large transition probabilities (log $gf > -0.8$) are in emission. They can be observed starting from Cr II at 6121.434 Å. All the identified Cr II emission lines are listed in Table A.5. The meaning of the columns is the same as in Table A.4. Fig. A.5 shows the Cr II emissions at 6285.241 Å and 6587.020 Å.

Sigut & Landstreet (1990) pointed out the large uncertainty affecting the Cr II log gfs. For the 4050-4650 Å interval, they reduced the discrepancies related to different sources by renormalising the Cr II oscillator strengths from Wujec & Weniger (1981) on a scale different from that adopted by Martin, Fuhr & Wiese (1988)(MFW). We adopted log gfs from MFW when the source is Kostyk & Orlova (1983) and from Sigut & Landstreet (1990) when the source is Wujec & Weniger (1981), except for Cr II $\lambda\lambda$ 4587.30, 4697.61 and 4715.12 Å. We kept log gfs from MFW for the three lines on the basis of the comparison of the observed and computed spectra. For Cr II at 4812.34 Å we adopted log $gf=-1.995$ from the Kurucz line lists in accordance with the discussion of Sigut & Landstreet (1990). For all the Cr II lines not considered by MFW we used log gfs from the Kurucz line lists without any renormalisation.

There are small wavelength differences in MFW and in the Kurucz line lists for a few Cr II lines. The wavelengths from Kurucz agree better with the observations. In several cases both the wavelengths from MFW and from the Kurucz line lists do not agree with the position of the observed lines. Examples are the Cr II lines at $\lambda\lambda$ 5308.46 Å, 5310.73 Å and 5313.61 Å, where the wavelengths are from MFW.

The average Cr I abundance is 0.2 dex larger than that from Cr II. The abundances are -5.22 ± 0.09 dex and -5.41 ± 0.07 dex, respectively. The average abundances from Cr II lines lying shortward and longward of the Balmer discontinuity are within the error limits. The average abundance from all the Cr I and Cr II lines is -5.36 ± 0.11 dex, corresponding to an overabundance of [+1.01].

Smith & Dworetsky (1993) obtained log(N(Cr)/N(H))$=-5.5\pm0.1$ from an IUE spectra analysis.

Manganese (25)-Mn I,Mn II: The spectrum is so rich in Mn I and Mn II lines that HD 175640 could be used as an ideal laboratory for studying the manganese spectrum.

The bulk of log gf data for Mn II lines comes from Kurucz (1992) computations, so that no spectral analyses of HgMn stars would be possible without the Kurucz data for this ion. Unfortunately, critical evaluations are unavailable for many of the Mn II lines, especially in the visible region.

There are numerous exceptionally broadened Mn II lines in the spectrum. This characteristic, which seems to be common to all HgMn stars, was first shown up by Jomaron, Dworetsky & Allen (1999), who explained it as due to hyperfine splitting. They were not fully able to reproduce the exceptionally broadened profiles owing to the lack of Mn II hyperfine structure experimental data. These measurements were made later on by Holt, Scholl & Rosner (1999), who confirmed the findings of Jamaron et al. (1999).

Isotope 25 is the only isotope of manganese. We added in the line lists the hyperfine components of several Mn II lines showing a large broadening in the spectrum. We adopted either the hyperfine log gfs taken from Holt et al. (1999) or we used the HYPERFINE code (Kurucz & Bell 1995) to compute hyperfine wavelengths and log gfs from the A and B hyperfine constants measured by Holt et al. (1999). Unfortunately, they cover only part of the Mn II levels.

The comparison of the wavelengths measured by Holt et al. (1999) with those from the Kurucz line lists has yielded non-negligible differences in some cases. The comparison of the observations with spectra computed with the two sets of wavelengths has favoured the Holt et al. (1999) data so that they were adopted in the line lists. Finally, in the Kurucz line lists the wavelengths of the lines of mult. 13 at 6122-6132 Å were replaced by the wavelengths measured by Johansson et al. (1995).

Table A.6 lists line data and (total or partial) hyperfine splitting for a large sample of Mn II lines. The multiplet number when available, the adopted wavelength, the adopted log gf, its source, the lower and upper excitation potentials in cm^{-1} and the total (or partial) hyperfine splitting hfs_{tot} are listed in successive columns. Here hfs_{tot} indicates the separation of the outermost components. Wavelengths marked with an asterisk were taken from Holt et al. (1999), while the others are from the Kurucz line lists. "hfs" just after the wavelength indicates that we added the hyperfine components of that line in the line lists. The hyperfine splitting hfs_{tot} listed in column 7 is total or partial according to whether the A and B constants are known for both levels or for only one of the levels involved in the transition. Some lines showing a large broadening in the observed spectrum, but lacking hyperfine data for computing the synthetic spectrum, are also listed in the table. Fig. 3 in the main paper shows the extreme hyperfine broadening which affects the Mn II lines at 7353.549 Å and 7415.803 Å. Other lines much broader than the computed ones are those at 9407.0 Å(Fig. A.2), 9408.7 Å and 9446.8 Å, in spite of the hyperfine splitting of the upper level being considered in the computations. The hyperfine splitting of their lower level is unknown and this is probably the reason for the disagreement.

No Mn II emission lines are observed in the spectrum but there are some lines in the red part of the spectrum which are much weaker than the predicted ones. This disagreement could be explained either with an superimposed emission or with wrong line data. The most remarkable features are those predicted at $\lambda\lambda$ 9867.0, 9903.836, 9904.464, 9905.269, 9906.221 and 9907.212 Å.

The Mn abundance log $(N(Mn)/N_{tot})=-4.20$, corresponding to [Mn/H]=+2.4, was derived from the measured equivalent widths (Table A.2) of both Mn I and Mn II lines having critically evaluated log gfs available in Martin, Fuhr & Wiese (1988). Therefore, for Mn II, only the lines of Mn II mult. 3 at 3464.0 Å were used. Hyperfine structure has negligible effects on these lines.

We have added in Table A.2 the abundances from the Mn II lines at $\lambda\lambda$ 3917.318, 4363.25, 4365.220 and 4478.637 Å, which were used by Jomaron et al. (1999) to study the Mn abundance in a given sample of HgMn stars. We excluded them from the averaged abundance determination. The average abundance from the four lines is -4.46 ± 0.06 dex. The discrepancy with the average abundance from the other examined lines amounts to -0.26 dex, which could be interpreted as an indication of manganese stratification. However, the log gf uncertainties prevent us from drawing any firm conclusion about manganese stratification insomuch that the average abundances from Mn I (-4.19 ± 0.10 dex) and Mn II (-4.25 ± 0.04 dex) are within the error limits. Also the differences between the average abundances from Mn I lines lying shortward and longward of the Balmer discontinuity are well within the error limits.

For comparison, we recall that the average abundances log(N(Mn)/N(H)) from Jomaron et al. (1999) are -4.44 ± 0.05 for Mn I and -4.54 ± 0.05 for Mn II. Smith et al. (1993) derived $\log(N(Mn)/N(H))=-4.35\pm0.05$ from the Mn II resonance lines at 2576 Å, 2593 Å, and 2605 Å measured in IUE spectra.

Iron (26)-Fe I,Fe II: The average Fe abundance from the equivalent widths of all the examined Fe I and Fe II lines (Table A.2) is $\log(N(Fe)/N_{tot})=-4.83\pm0.13$, corresponding to an underabundance of [−0.3]. The average abundance from Fe I lines, -4.78 ± 0.08 dex, agrees within the error limits with the average abundance from Fe II lines, -4.84 ± 0.13 dex, while the abundances from the Fe I lines shortward and longward of the Balmer discontinuity differ by 0.15 dex, which is more than the error limits. Lines lying in the near UV give the lower abundance value. The Fe II abundance from this study is the same as that derived by Hubrig & Castelli (2001) using only the equivalent width of the Fe II line at 6149.258 Å measured in a spectrum observed at CFHT.

Smith & Dworetsky (1993) found log(N(Fe)/N(H))= −5.05±0.05 from the analysis of IUE spectra.

Cobalt (27)-Co II (Not observed ?): No cobalt lines were observed in the UVES spectra, except for Co II mult. 2 at 3501.717 Å, which could also be noise as well. The computed profile reproduces the observed spectrum for an abundance log(N(Co)/N_{tot})=−8.08, which is about ten times lower than the solar abundance. We adopted the above value.

Smith & Dworetsky (1993) derived an upper limit log(N(Co)/N(H))≤−9.0±0.5 from an IUE spectra analysis.

Nickel (28)-Ni II: The equivalent widths of the measured Ni II lines (Table A.2) give an underabundance [−0.3] if log gfs recomputed by Kurucz (2003) are used for all the lines examined (Table A.2). Instead, if log gfs from Heise (1974) are used, the nickel underabundance changes from [−0.3] to [−0.8]. There are no Ni II critically evaluated log gfs in the NIST database for the whole wavelength region studied by us. We adopted the abundance log(N(Ni)/N_{tot})=−6.09±0.16, which is that based on the Kurucz (2003) log gfs. Smith & Dworetsky (1993) found log(N(Ni)/N(H))=−6.2±0.3 from their analysis of IUE spectra.

Copper (29)-Cu I: While no Cu II lines were observed, the Cu I line at 3247.540 Å was measured. It is probably blended with some unknown component, as it is asymmetric, with a more extended red wing. In fact, the abundance −6.52 dex from the equivalent width 5.96 mA gives a too strong computed profile. On the basis of the synthetic spectrum we adopted log(N(Cu)/N_{tot})=−6.88, corresponding to an overabundance of [+0.95]. This value well reproduces also Cu I 3273.954 Å which is blended with Mn II 3274.044 Å.

Smith (1994) derived log(N(Cu)/N(H))=−6.85±0.15 from Cu II lines observed in IUE spectra.

Zinc (30)-Not observed: No zinc lines were observed. Smith (1994) found log(N(Zn)/N(H))=−9.22±0.30 from Zn II lines observed in IUE spectra. This corresponds to an underabundance [−1.8].

Gallium (31)-Ga I,Ga II: There are only two Ga I lines in the studied range with available log gfs in the NIST database. They are Ga I mult. 1 at 4032.990 Å and 4172.039 Å. Both lines were observed in the spectrum, but they were not measured owing to their blending with other lines. Other Ga I lines can be found in the Kurucz line lists with guessed log gf values. The line at 6396.560 Å, if present, is heavily blended with Mn II 6396.565 Å.

There are no Ga II lines in the Kurucz line lists and there are no Ga II log gfs in the NIST database for the studied region. We used the Isberg & Litzén (1985) Ga II line list to identify Ga II lines in the spectrum and we searched the literature for Ga II oscillator strengths. The most complete set of log gfs in the optical region is that from Ryabchikova & Smirnov (1994) who consider 12 Ga II lines. However, the log gf uncertainty can be estimated when different determinations are compared. For instance, for the line at 6334 Å there is the choice between log gf=+1.00 from Ryabchikova & Smirnov (1994) and log gf=+0.36 from Lanz et al. (1993), while for the line at 5421.275 Å the log gf value is +0.55 according to Ryabchikova & Smirnov (1994) and −0.05 according to Nielsen, Karlsson & Wahlgren (2000). The comparison of the observed and computed profiles has led us to adopt +1.00 in the first case and −0.05 in the second case. In general, we adopted the Nielsen et al. (2000) log gfs, which are the same as those given by Ryabchikova & Smirnov (1994) for almost all the analyzed lines. For the transitions at 4255 Å we separated the 4255.722 Å and 4255.937 Å contributions. We replaced the global log gf=+0.68 with log gf=+0.634 and log gf=−0.320, respectively (Nielsen et al. 2000).

Several Ga II profiles are affected by isotopic and hyperfine broadening. Ga II in HgMn stars was discussed by Nielsen, Karlsson & Wahlgren (2000) and by Dworetsky, Jomaron & Smith (1998). Gallium has two stable isotopes Ga^{69} and Ga^{71} with relative terrestrial abundances 0.60108 and 0.39892 (Anders & Grevesse 1989). Lines from each isotope are affected by hyperfine splitting of the levels. Karlsson & Litzèn (2000) measured the isotopic and the hyperfine structure of 18 Ga II lines by means of Fourier transform spectroscopy. They obtained hyperfine A constants for 8 levels. The B constants were found to be close to zero. We used the A constants in the HYPERFINE code (Kurucz & Bell 1995) to compute hyperfine log gfs for 8 lines with λ>5000 Å. Their hyperfine and isotopic wavelengths were taken from Karlsson & Litzèn (2000). For 7 Ga II lines at 4251-4263 Å, arising from the 4d-4f transition, Karlsson & Litzèn (2000) measured the wavelengths and the relative intensities of numerous components. We estimated the log gf of each component from the ratio of the intensity of the component to the total intensity of the components. We did not use the standard formulae of the LS coupling (Cowley et al. 2000) owing to the lack in Table 3 of Karlsson & Litzén (2000) of the F total angular momentum for the lower and upper level of the transitions.

The Ga II isotopic and hyperfine components that we derived from Karlsson & Litzèn (2000) for 15 Ga II lines are listed in Table A.7. We included them in the Kurucz line lists. Table A.7 is formed by subtables, one for each line investigated. The wavelength and the log gf of the examined transition are given in italics at the top of each subtable. The wavelengths of the isotopic and hyperfine components follow. They are listed in col. 2 in increasing wavelength order. Col. 3 and col. 4 show the oscillator strengths of the isotopic and hyperfine components, log gf_{iso} and log gf_{hfs}, respectively. The total oscillator

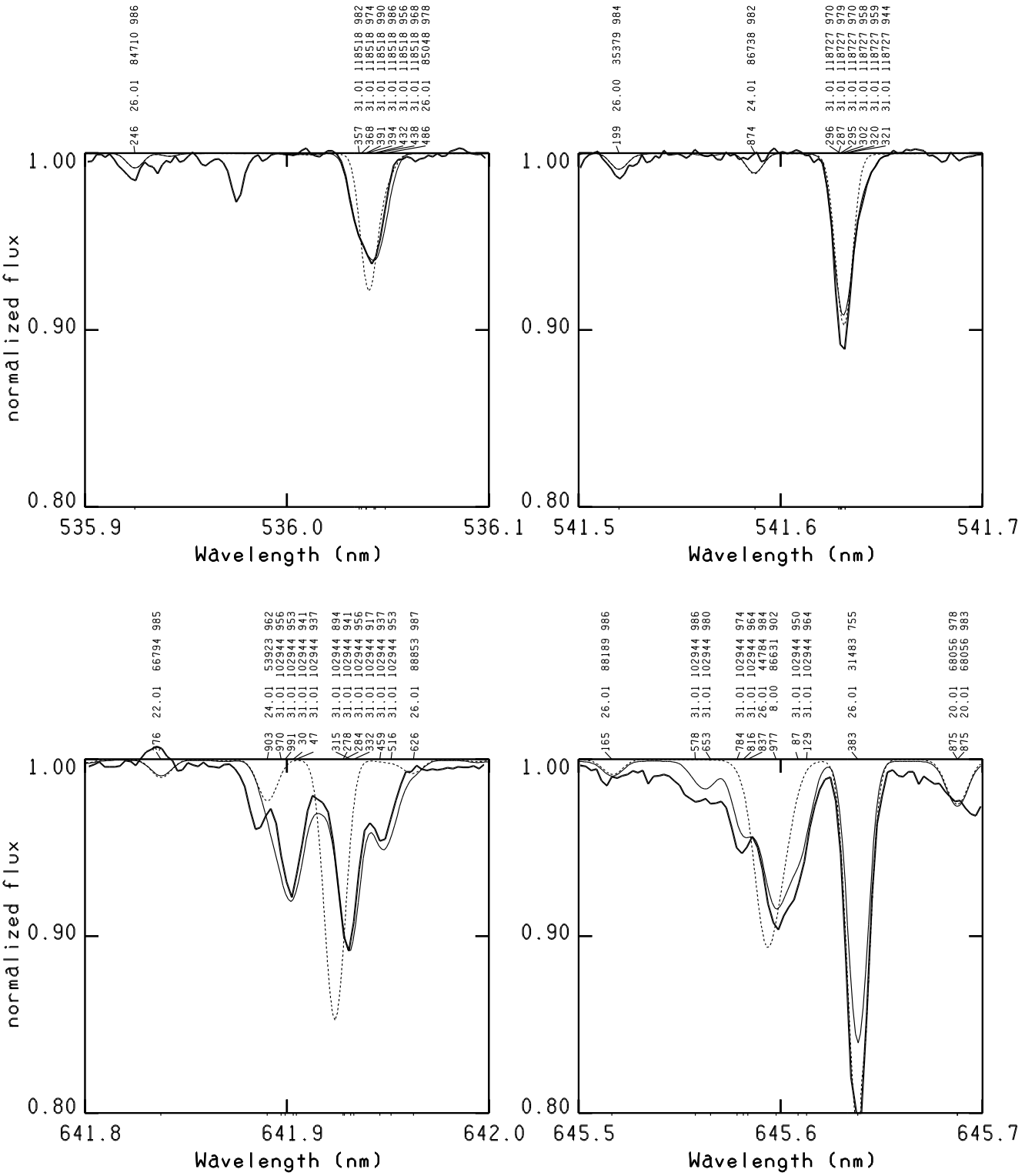

Fig. A.6. The observed profiles (thick full lines) of Ga II at $\lambda\lambda$ 536.03, 541.63, 641.89, 641.93, and 645.65-645.68 nm are compared with synthetic profiles computed once without any hyperfine structure (dotted lines) and once with hyperfine structure included in the computations (thin full lines) The meaning of the identification labels is the same as that given in the caption of Fig. A.1

strength of each component, log $gf_{\rm comp}$, is given in the last column. It was obtained by summing the log gf of the whole transition with log $gf_{\rm iso}$ and log $gf_{\rm hfs}$.

The Ga II lines analyzed in HD 175640, their log gf, the source, and the abundances derived from the line profiles are shown in Table A.3. The average abundance is log(N(Ga)/$N_{\rm tot}$)=$-$5.43$\pm$0.04, corresponding to an overabundance [+3.73]. A few other Ga II lines not used for abundance purposes have been added to Table A.3. Their log gf is that which gives the best agreement between

the observed and computed profiles for the adopted abundance.

The analysis of the individual Ga II lines shows that the observed Ga II profile at λ 4251 Å is slightly broader and stronger than that computed for the adopted −5.43 dex abundance. A similar behaviour was pointed out by Nielsen et al. (2000) in κ Cnc and in HR 7775. The line could be blended with an unknown blue absorption line. The observed Ga II profile at λ 4255.7-4255.9 would be better reproduced if the predicted Mn II at 5256.014 Å is dropped. The observed and computed profiles of the blend Cr II 4261.9 Å, Ga II 4262.0 Å agree rather well. Although hfs and isotopic structures are not well evident in the Ga II lines observed at 5338.24 Å, 5360.40 Å, 5363.58 Å, 5416.31 Å and 5421.27 Å, the synthetic profiles reproduce well the observed ones only when the fine structures are considered in the computations. Large structures due to the isotopic and hyperfine splittings can be observed in the lines at 6334 Å, 6419 Å and 6456 Å. Fig. A.6 compares each of the profiles observed at 5360.4 Å, 5421.3 Å, 6419.0 Å and 6456.0 Å with two synthetic profiles, one computed with isotopic and hyperfine structures, the other without them.

Dworetsky et al. (1998) obtained log(N(Ga)/N(H))= −5.36±0.14 for this star.

Arsenic (33)-As II (Not observed ?): Sadakane et al. (2001) identified in the 5100-6400 Å region of the HgMn stars 46 Aquilae eight absorption features at 5105.58 Å, 5107.55 Å, 5231.38 Å, 5331.23 Å, 5497.73 Å, 5558.09 Å, 5651.32 Å and at 6110.07 Å as As II. We observed weak unidentified features in HD 175640 only at 5331.23 Å, 5497.73 Å, 5558.09 Å and 5651.32 Å. Other As II lines listed in the NIST database, even with stronger intensities, are not detectable in the spectrum. This suggests that other elements than As II may produce the four weak unidentified lines. We did not find in the literature any log gf for As II in the visible region.

Bromine (35)-Br II: Only the three Br II lines at 4704.85 Å, 4785.50 Å and 4816.70 Å have log gf values in the NIST database. We measured the equivalent widths of the first two lines, which yielded a Br overabundance of [+2.3].

Strontium (38)-Sr II: Only few Sr II lines were identified in the spectrum. The equivalent width of the unique Sr II unblended line at 4077.71 Å yields log (N(Sr)/N_{tot})=−8.41, corresponding to an overabundance of [+0.7]. This value correctly reproduces the other observed Sr II blended lines, in particular the blend at 4215.5 Å having Sr II λ 4215.52 Å as main component.

Yttrium (39)-Y II: Although numerous Y II unblended lines were identified in the spectrum on the basis of the Kurucz line lists, only half of them could be used for abundance purposes, owing to the lack of log gf values for a large number of Y II transitions. Lines with unknown log gfs have guessed values in the Kurucz line lists so that the predicted lines in the synthetic spectrum have fictitious intensities.

The most reliable log gf source is Hannaford et al. (1982), who provided experimental values. Some other log gfs in the Kurucz line lists were obtained from a fitting procedure from Cowley & Corliss (1983). However, log gfs of lines with energy levels lying outside the validity range of the fitting procedure predict lines so much stronger than the observed ones that they should be considered unreliable values.

Nilsson, Johansson & Kurucz (1991) have measured Y II wavelengths in the region 1000-48800 Å. We added a few lines from Nilsson et al. (1991) in the Kurucz line lists and assigned guessed log gfs to them. We also replaced a few wavelengths in the Kurucz database with wavelengths measured by Nilsson et al. (1991) as they agree better with the position of the observed lines.

The average abundance from the equivalent widths of the lines listed in Table A.3 is log(N(Y II)/N_{tot})= −6.66±0.20, corresponding to [Y/H]=+3.14. However, there is a difference of 0.4 dex between the average abundances derived from lines lying shortward or longward of the Balmer discontinuity. These abundances are −6.42±0.06 dex and −6.79±0.10 dex, respectively.

Zirconium (40)-Zr II: Only a few weak Zr II lines were identified. From the equivalent widths listed in Table A.3 we derived an overabundance [Zr/H]=+0.77.

Rhodium (45)-Rh II: We identified all the Rh II lines listed in Table A.3. Owing to the lack of log gfs for them, we used the guessed oscillator strengths from the Kurucz line lists. Assuming log gf=0.00 for Rh II at λ 3233.314 Å the abundance is −8.50 dex, viz. Rh II should be overabundant by about [+2.4]. The wavelengths in the Kurucz line lists are slightly different from those given in the Moore (1972) tables. The observed wavelengths correspond better with the Moore than to the Kurucz data. When needed, we modified the wavelengths in the Kurucz line lists to match the position of the observed lines. For the lines embedded in blends the wavelengths from Moore (1972) were adopted.

Palladium (46)-Pd I, Pd II: Several very weak Pd I lines included in the Kurucz line lists were identified in the spectrum. The measured equivalent widths (Table A.3) give an average overabundance [+3.94].

The log gf sources in the Kurucz database are Biémont et al. (1981) and Corliss & Bozman (1962).

We did not identify Pd II owing to the lack of these lines in our line lists. However, as pointed out by the referee dr. C.R. Cowley, they were identified in HD 175640 by Bord et al. (2003)[1]. Two Pd II lines can be seen as uniden-

[1] http://www.astro.lsa.umich.edu/users/cowley/AAS0503Don/P7143.htm

tified features in our synthetic spectrum at 3243.1 Å and 3267.4 Å.

Xenon (54)-Xe II: Numerous Xe II lines were identified in the spectrum. Because no Xe II lines are included in the Kurucz line lists, we added all the Xe II lines available in Wiese & Martin (1980). From lines with measurable equivalent widths (Table A.3) we obtained $\log(N(Xe)/N_{tot})=-5.96\pm0.20$, corresponding to an overabundance [Xe/H]=+3.87 dex. We added in Table A.3 some other weak Xe II lines with no measurable equivalent widths, but which are well reproduced in the synthetic spectrum by the above abundance. We also added in Table A.3 a few other Xe II lines observed in the spectrum. Their wavelengths and energy levels were taken from Hansen & Persson (1987). We assigned a fictitious $\log gf=0.00$ to them to be able to compute an approximate profile in the synthetic spectrum.

Barium (56)-Ba II: Only two very weak Ba II lines at 4554.03 Å and 4934.08 Å were identified in the spectrum.

Barium has seven isotopes, Ba^{130}, Ba^{132}, Ba^{134}, Ba^{135}, Ba^{136}, Ba^{137} and Ba^{138}. The stable ones are those with mass numbers 134 to 138. The lines of odd isotopes of Ba are affected by hyperfine structure. We considered all the isotopic and hyperfine components for computing the Ba II profile at 4554.03 Å. They are listed in Table A.8. The hfs components were computed with the HYPERFINE code (Kurucz & Bell 1995) using the hyperfine constants A and B taken from Becker & Werth (1983) and Becker et al. (1968). The isotopic intensities are from Anders & Grevesse (1989). The wavelength and the $\log gf$ of the whole transition were taken from Miles & Wiese (1969). However, the line at λ 4554.03 Å is so weak in HD 175640 that hyperfine and isotopic broadenings do not contribute to the profile in a significant way. The abundance from this profile is $\log(N(Ba)/N_{tot})=-9.27$, which corresponds to an overabundance [+0.64].

Cerium (58)-Not observed ?: Numerous Ce II lines are considered in the Kurucz line lists, but no Ce III lines. We added to the Kurucz line lists only those Ce III lines which were studied by Bord et al. (1997), but we adopted the $\log gf$ values available in the DREAM database.

No Ce III lines can be identified in the spectrum, although some weak Ce II lines could be present (i.e. λ 5079.682). The abundance $\log(N(Ce)/N_{tot})=-7.8$ derived from Ce II predicts very strong unobserved Ce III lines. We assumed Ce solar abundance for computing the synthetic spectrum although a large overabundance of Ce II compared to that of Ce III cannot be excluded.

Praseodymium (59)-Pr III: There are numerous Pr II lines in the Kurucz line lists, but none of Pr III. We added only those Pr III lines which were studied by Dolk et al. (2002), but we adopted the $\log gf$ values from Biémont et al. (2001b) for them.

No lines of Pr II were observed, but lines of Pr III may be present. With the aid of the synthetic spectrum we identified Pr III lines at 5264.433 Å, 5299.969 Å and 7781.985 Å. The abundance which fits the profile of the second unblended line is $\log(N(Pr)/N_{tot})=-9.62$, corresponding to an overabundance [Pr/H]=+1.7. This is not in conflict with the predicted intensity of the first line which is blended with Mg II and with that of the last line, which is at the level of the noise. However, other weak Pr III lines with no observed counterparts are predicted for this abundance.

Neodymium (60)-Nd III: There are numerous Nd II lines in the Kurucz line lists, but none of Nd III. We added only those Nd III lines which were studied by Dolk et al. (2002), but we adopted the $\log gf$ values from Zhang et al. (2002), available in the DREAM database.

We identified weak lines of Nd III at $\lambda\lambda$ 5102.455, 5127.044, 5203.902 and 5203.924 Å. They are rather well reproduced by the abundance $\log(N(Nd)/N_{tot})=-9.60$, corresponding to an overabundance [Nd/H]=+0.94. Weak Nd III absorption features not in conflict with the observations are predicted for this abundance at 4903.241 Å and 4927.488 Å.

Ytterbium (70)-Yb II,Yb III: Among the REE, only Yb II and Yb III have been identified without any doubt in this star (Bord et al. 2003).

There are numerous Yb II lines in the Kurucz line lists, but none of Yb III. We added Yb III lines from Biémont et al. (2001a) and replaced the Yb II $\log gf$s of the Kurucz line lists with those from Biémont et al. (1998). All the Biémont et al. (2001a; 1998) $\log gf$s were taken from the DREAM database.

The average abundance from the Yb II equivalent widths is $\log(N(Y)/N_{tot})= -8.10\pm0.19$ (Table A.3). If $\log gf$s from the Kurucz database are used, the abundance is -8.31 ± 0.16. The average abundance from the Yb III equivalent widths is $\log(N(Yb)/N_{tot})=-7.3$, namely 0.7 dex higher than that from Yb II (Table A.3). The synthetic spectrum was computed with $\log(N(Yb)/N_{tot})= -8.10$.

Osmium (76)-Os II: Only four Os II lines are available in the Kurucz line lists for the studied region. They lie shortward of the Balmer discontinuity. The line at 3173.931 Å is predicted in the synthetic spectrum for solar abundance. It is a very weak line not in conflict with the observed spectrum.

Iridium (77)-Ir II: Only the line of Ir II at 3042.553 Å is available in the Kurucz line lists for the studied region. The line profile computed for a solar iridium abundance agrees well with the observed spectrum.

Platinum (78)-Pt II We investigated the presence in the spectrum of the Pt II lines listed by Engleman(1989). Two lines were identified, λ 4061.644 Å and λ 4514.124 Å. The first produces an asymmetric profile centered at the position of Fe II λ4061.782Å, the second can be unambigously observed.

There are no Pt II lines in the Kurucz line lists. We added the seven Pt II lines for which astrophysical log gfs from Dworetsky et al. (1984) are available. For the lines at 4046.443 Å, 4288.371 Å, and 4514.124 Å we also considered the isotopic and hyperfine wavelengths from Engleman (1989) together with the isotopic composition from Anders & Grevesse (1989). From the line profile at 4514.124 Å we obtained a Pt II abundance of −7.63 dex, corresponding to an overabundance [+2.57].

The line at λ 4061.644 Å computed for the above abundance contributes to the observed blend, but the line predicted at λ 4046.443 Å is not observed. There are also very weak predicted Pt II lines with no observable counterparts at $\lambda\lambda$ 4288.371 Å and 4034.181 Å.

Unfortunately, we did not find neither experimental nor theoretical log gfs for Pt II lines lying shortward of the Balmer discontinuity.

Gold (79)-Au II: There are no Au II lines in the Kurucz line lists. We added the Au II lines from Rosberg & Wyart (1997) for the range 3040-10000 Å.

We identified and measured the equivalent widths of two lines at 4016.672 and 4052.790 Å, respectively. The average abundance is $\log(N(Au)/N_{tot})=-7.51\pm0.06$, corresponding to an overabundance [Au/H]=+3.52.

Mercury (80)-Hg I, Hg II: For λ>4000 Å we replaced log gfs of the Kurucz line lists with the log gfs from Benck et al. (1989) for Hg I. We took wavelengths and log gfs from Sansonetti & Reader (2001) for Hg II. Only for the Hg II line at 3984 Å did we adopt log gf=−1.520, which is the mean value of −1.529 dex from Proffitt et al. (1999) and −1.510 dex from Sansonetti & Reader (2001).

Mercury has seven isotopes: 196, 198, 199, 200, 201, 202 and 204. The isotopes 199 and 201 are affected by hyperfine splitting. We considered all the isotopic and hyperfine components for computing Hg I at 4358 Å and Hg II at 3984 Å and 6149 Å. They are listed in Table A.9 The hyperfine oscillator strengths were taken from Dolk et al. (2003). The mercury isotopic composition of HD 175640 was derived from Hg II at 3984 Å by assuming $\log(N(Hg)/N_{tot})=-6.30$. It is very different from the terrestrial one and very close to that found by Dolk et al. (2003). We recall that the terrestrial log gf_{iso} values of the isotopes 196, 198, 199, 200, 201, 202 and 204 are −2.814, −1.001, −0.773, −0.636, −0.880, −0.525 and −1.163, respectively (Anders & Grevesse 1989).

The abundance −6.30 dex that we derived from Hg II at λ 3984 Å was used to compute the synthetic spectrum. Four Hg I lines at 3125.665 Å, 4046.56 Å, 4358.3 Å, and 5460.73 Å and five Hg II lines at 3984 Å, 5425.253 Å 5677.105 Å, 6149 Å, and 7944.555 Å are predicted for this abundance. The computed profiles of the first three Hg I lines are slightly stronger than the observed ones, while Hg I at 5460.731 Å is predicted weaker than observed. The line of Hg II at 5425.253 Å is heavy blended with Fe II λ 5425.257 Å. The whole predicted blend is stronger than the observed one. Hg II at 5677.105 Å and 7944.555 Å are not observed but they are predicted in the synthetic spectrum. Finally, the computed line of Hg II at 6149.475 Å is slightly stronger than the observed one.

We could conclude that, except for Hg I at 5460.731 Å, the abundance derived from Hg II λ 3984 Å is too large in spite of its agreement with that found by Dolk et al. (2003), which is $\log(N(Hg)/N_{tot})=-6.35\pm0.15$. Furthermore, this abundance is lower than that derived by Smith (1997) from Hg II at 1942 Å, which was estimated to lie between −6.25 and −6.15 dex.

Table A.1. Abundances of the light elements.

Mult.	λ(Å)	log gf	Ref.[a]	χ_{low}(cm^{-1})	log γ_S/N$_e$	Ref.[b]	W(mÅ)	$log(N_Z/N_{\rm tot})$	Notes
		He I	logN(He I)/N$_{\rm tot}$=−1.73						
88 (22)	3819.6020	−2.968	NIST	169086.87		DS90		−1.73	
88 (22)	3819.6028	−1.045	NIST	169086.87		DS90		−1.73	
88 (22)	3819.6028	−1.794	NIST	169086.87		DS90		−1.73	
88 (22)	3819.6131	−1.794	NIST	169086.95		DS90		−1.73	
88 (22)	3819.6139	−1.315	NIST	169086.95		DS90		−1.73	
88 (22)	3819.7573	−1.668	NIST	169087.93		DS90		−1.73	
82 (20)	3867.4723	−2.055	NIST	169086.87		DS90		−1.73	
82 (20)	3867.4837	−2.276	NIST	169086.95		DS90		−1.73	
82 (20)	3867.6315	−2.754	NIST	169087.93		DS90		−1.73	
32 (58)	3926.5443	−1.647	NIST	171155.00		DS90		−1.73	not observed
31 (55)	4009.2565	−1.473	NIST	171135.00		DS90		−1.73	not observed
25 (54)	4023.9798	−2.577	NIST	171135.00		DS90		−1.73	on the wing of He I 4026
87 (18)	4026.1844	−2.625	NIST	169086.87		SM69		−1.73	bad fit for the blue wing
87 (18)	4026.1859	−1.448	NIST	169086.87		SM69		−1.73	
87 (18)	4026.1860	−0.701	NIST	168086.87		SM69		−1.73	
87 (18)	4026.1968	−1.449	NIST	169086.95		SM69		−1.73	
87 (18)	4026.1983	−0.972	NIST	169086.95		SM69		−1.73	
87 (18)	4026.3570	−1.324	NIST	169087.93		SM69		−1.73	
81 (16)	4120.8108	−1.738	NIST	169086.87		G74		−1.73	on the red wing of Hδ
81 (16)	4120.8237	−1.961	NIST	169086.95		G74		−1.73	
81 (16)	4120.9916	−2.437	NIST	169087.93		G74		−1.73	
30 (53)	4143.7590	−1.196	NIST	171135.00		DS90		−1.73	not observed
24 (52)	4168.9716	−2.338	NIST	171135.00		DS90		−1.73	not observed
29 (51)	4387.9291	−0.883	NIST	171135.00		SM69		−1.73	
23 (50)	4437.5536	−2.034	NIST	171135.00		G74		−1.73	
86 (14)	4471.4704	−2.203	NIST	169086.87		BCS1		−1.73	
86 (14)	4471.4741	−1.026	NIST	169086.87		BCS1		−1.73	
86 (14)	4471.4743	−0.278	NIST	169086.87		BCS1		−1.73	
86 (14)	4471.4856	−1.025	NIST	169086.95		BCS1		−1.73	
86 (14)	4471.4893	−0.550	NIST	169086.95		BCS1		−1.73	
86 (14)	4471.6832	−0.903	NIST	169087.93		BCS1		−1.73	
80 (12)	4713.1392	−1.230	NIST	169086.87		G74		−1.73	blend with Cr II, Fe II
80 (12)	4713.1562	−1.452	NIST	169086.94		G74		−1.73	
80 (12)	4713.3757	−1.928	NIST	169087.93		G74		−1.73	
28 (48)	4921.9310	−0.435	NIST	171135.00		BCS2		−1.73	
13 (4)	5015.6776	−0.820	NIST	166277.54		G74		−1.73	blend with Fe II
22 (47)	5047.7384	−1.601	NIST	171135.00		G74		−1.73	blend with Fe II
85 (11)	5875.5987	−1.516	NIST	169086.87		G74		−1.73	
85 (11)	5875.6139	−0.341	NIST	169086.87		G74		−1.73	
85 (11)	5875.6148	+0.408	NIST	169086.87		G74		−1.73	
85 (11)	5875.6251	−0.340	NIST	169086.95		G74		−1.73	
85 (11)	5875.6403	+0.137	NIST	169086.95		G74		−1.73	
85 (11)	5875.9663	−0.215	NIST	169087.93		G74		−1.73	
27 (46)	6678.1517	+0.329	NIST	171135.00		G74		−1.73	
79 (10)	7065.179	−0.461	NIST	169086.87		G74		−1.73	
79 (10)	7065.217	−0.682	NIST	169086.95		G74		−1.73	
79 (10)	7065.710	−1.160	NIST	169087.93		G74		−1.73	
		Be II	logN(Be II)/N$_{\rm tot}$=−10.64						
1	3130.420	−0.168	K,BIE	0.00	−5.80	G74 (K)	7.12	−10.64	
		C I	logN(C I)/N$_{\rm tot}$=−4.11±0.23						
6	4771.747	−1.866	CNO	60393.14	−4.59	G74	1.58	−3.82	
13	4932.049	−1.658	CNO	61981.82	−4.32	G74	1.19	−4.05	
3	9062.487	−0.456	CNO	60333.43	−5.32	G74	24.41	−3.98	
3	9111.807	−0.298	CNO	60393.14	−5.32	G74	21.88	−4.19	
2	9603.034	−0.896	CNO	60333.43	−5.40	G74	3.05:	−4.49	
		C II	logN(C II)/N$_{\rm tot}$=−4.05±0.16						
4	3918.968	−0.533	CNO	131724.37	−4.93	G74	12.23	−3.95	
6	4267.261	+0.717	CNO	145550.70	−4.76	G74	22.57	−3.87	
2	6578.052	−0.026	CNO	116537.65	−5.35	G74	8.68	−4.31	on the wing of H$_\alpha$
2	6582.882	−0.328	CNO	116537.65	−5.35	G74	7.60	−4.08	on the wing of H$_\alpha$

Table A.1. Abundances of the light elements, cont.

Mult.	λ(Å)	log gf	Ref.[a]	χ_{low}(cm^{-1})	log(γ_S/N$_e$)	Ref.[b]	W(mÅ)	$log(N_Z/N_{\rm tot})$	Notes
		O I	log N(O I)/N$_{\rm tot}$=−3.18±0.11						
3	3947.295	−2.096	CNO	73768.20	−4.70	G74	6.54	−3.40	
3	3947.481	−2.244	CNO	73768.20	−4.70	G74		−3.40	
3	3947.586	−2.467	CNO	73768.20	−4.70	G74		−3.40	
5	4368.190	−2.665	CNO	76794.98	−4.68	G74		−3.20	
5	4368.242	−1.964	CNO	76794.98	−4.68	G74		−3.20	
5	4368.258	−2.818	CNO	76794.98	−4.68	G74		−3.20	
14	4967.380	−2.086	CNO	86625.76	−−	−−			no fit
14	4967.380	−1.997	CNO	86625.76	−−	−−			no fit
14	4967.380	−2.329	CNO	86625.76	−−	−−			no fit
14	4967.880	−1.660	CNO	86627.78	−−	−−			no fit
14	4967.880	−1.865	CNO	86627.78	−−	−−			no fit
14	4967.880	−2.454	CNO	86627.78	−−	−−			no fit
14	4968.790	−1.375	CNO	86631.45	−−	−−			no fit
14	4968.790	−1.961	CNO	86631.45	−−	−−			no fit
14	4968.790	−2.087	CNO	86631.45	−−	−−			no fit
13	5020.218	−1.725	CNO	86631.45	−−	−−	2.87	−3.35	
12	5329.096	−1.938	CNO	86625.76	−3.43	G74		−3.27	
12	5329.099	−1.586	CNO	86625.76	−3.43	G74		−3.27	
12	5329.107	−1.695	CNO	86625.76	−3.43	G74		−3.27	
12	5329.673	−2.063	CNO	86627.78	−3.43	G74		$\leq$−3.27	blend with Mn II
12	5329.681	−1.473	CNO	86627.78	−3.43	G74		$\leq$−3.27	blend with Mn II
12	5329.690	−1.269	CNO	86627.78	−3.43	G74		$\leq$−3.27	blend with Mn II
12	5330.735	−1.570	CNO	86631.45	−3.43	G74		−3.27	
12	5330.741	−0.984	CNO	86631.45	−3.43	G74		−3.27	
11	5435.178	−1.766	CNO	86625.76	−3.82	G74	4.20	−3.20	
11	5435.775	−1.544	CNO	86627.78	−3.82	G74	5.99	−3.16	
11	5436.862	−1.398	CNO	86631.45	−3.82	G74	7.49	−3.20	
10	6155.961	−1.363	CNO	86625.76	−3.96	G74		−3.17	
10	6155.971	−1.011	CNO	86625.76	−3.96	G74		−3.17	
10	6155.989	−1.120	CNO	86625.76	−3.96	G74		−3.17	
10	6156.737	−1.488	CNO	86627.78	−3.96	G74		−3.17	
10	6156.755	−0.899	CNO	86627.78	−3.96	G74		−3.17	
10	6156.778	−0.694	CNO	86627.78	−3.96	G74		−3.17	
10	6158.149	−1.841	CNO	86631.45	−3.96	G74		−3.17	blend with Cr II, Cr II
10	6158.172	−0.996	CNO	86631.45	−3.96	G74		−3.17	blend with Cr II, Cr II
10	6158.187	−0.409	CNO	86631.45	−3.96	G74		−3.17	blend with Cr II, Cr II
9	6453.602	−1.288	CNO	86625.76	−4.28	G74	7.34	−3.24	
9	6454.444	−1.066	CNO	86627.78	−4.28	G74	11.95	−3.23	
9	6455.977	−0.920	CNO	86631.45	−4.28	G74		(−3.27)	blend with Ga II
21	7001.899	−1.489	CNO	88630.59	−3.93	G74		−3.27	blend with Mn II
21	7001.922	−1.012	CNO	88630.59	−3.93	G74		−3.27	blend with Mn II
21	7002.173	−2.644	CNO	88631.15	−3.93	G74		−3.22	
21	7002.196	−1.489	CNO	88631.15	−3.93	G74		−3.22	
21	7002.230	−0.741	CNO	88631.15	−3.93	G74		−3.22	
21	7002.250	−1.364	CNO	88631.30	−3.93	G74		−3.22	
38	7156.701	+0.288	CNO	102662.03	−5.35	G74	23.70	−3.11	
1	7771.944	+0.369	CNO	73768.20	−5.55	G74	190.78	−2.04	no fit
1	7774.166	+0.223	CNO	73768.20	−5.55	G74	174.48	−2.08	no fit
1	7775.388	+0.001	CNO	73768.20	−5.55	G74	148.12	−2.20	no fit
35	7947.548	+0.500	K,NBS	101135.41	−5.54	G74	32.22	−3.02	
35	7950.803	+0.340	K,NBS	101147.53	−5.54	G74	25.98	−3.09	
35	7952.159	+0.170	K,NBS	101155.42	−5.54	G74	21.46	−3.14	
34	8221.824	+0.313	CNO	101135.41	−5.40	G74		−3.10	
4	8446.247	−0.463	CNO	76794.98	−5.44	G74			no fit
4	8446.359	+0.236	CNO	76794.98	−5.44	G74			no fit
4	8446.758	+0.014	CNO	76794.98	−5.44	G74			no fit
37	8820.423	+0.379	CNO	102662.03	−5.51	G74	43.43	−3.04	
8	9260.806	−0.242	CNO	86625.76	−4.95	G74			no fit
8	9260.848	+0.110	CNO	86625.76	−4.95	G74			no fit
8	9260.848	+0.001	CNO	86625.76	−4.95	G74			no fit

Table A.1. Abundances of the light elements, cont.

Mult.	λ(Å)	log gf	Ref.[a]	χ_{low}(cm^{-1})	log(γ_S/N$_e$)	Ref.[b]	W(mÅ)	$log(N_Z/N_{\rm tot})$	Notes
			O I cont.						
8	9262.582	−0.367	CNO	86627.78	−4.95	G74			no fit
8	9262.670	+0.223	CNO	86627.78	−4.95	G74			no fit
8	9262.776	+0.427	CNO	86627.78	−4.95	G74			no fit
8	9265.826	−0.719	CNO	86631.45	−4.95	G74			no fit
8	9265.932	+0.126	CNO	86631.45	−4.95	G74			no fit
8	9266.006	+0.712	CNO	86631.45	−4.95	G74			no fit
			Ne I log N(Ne I)/N$_{\rm tot}$=−4.35						
1	7032.413	−0.294	NIST	134041.840	−6.32	G74	2.23	−4.35	
			Na I log N(Na I)/N$_{\rm tot}$=−5.47						
6	5688.205	−0.450	K,KP	16973.37	−5.68	G74		−5.47:	blend with telluric lines
1	5889.950	+0.112	NIST	0.00	−5.64	G74		−5.47:	blend interstell./circumstell. line
1	5895.924	−0.191	NIST	0.00	−5.64	G74		−5.47:	blend interstell./ circumstell. line
4	8183.255	+0.260	NIST	16956.17	−5.52	G74		$\geq$−5.47:	blend with telluric line
4	8194.790	−0.441	NIST	16973.37	−5.52	G74		−5.47	
4	8194.824	+0.514	NIST	16973.37	−5.52	G74		−5.47	
			Mg I log N(Mg I)/N$_{\rm tot}$=−4.64±0.06						
40	4702.991	−0.374	NIST	35051.26	−3.98	G74	2.09	−4.72	
2	5167.321	−0.856	NIST	21850.41	−5.27	G74	5.80	−4.57	
2	5172.684	−0.380	NIST	21870.46	−5.27	G74	13.74	−4.63	
2	5183.604	−0.158	NIST	21911.18	−5.27	G74		−4.58	blend with Fe II,Ti II
			Mg II log N(Mg II)/N$_{\rm tot}$=−4.71±0.07						
10	4384.637	−0.792	NIST	80619.50	−4.02	G74	24.11	−4.81	
10	4390.514	−1.706	NIST	80650.02	−4.02	G74	39.57	−4.76	
10	4390.572	−0.530	NIST	80650.02	−4.02	G74	39.57	−4.76	
9	4427.994	−1.201	NIST	80619.50	−4.40	G74	13.44	−4.70	
4	4481.126	+0.730	NIST	71490.19	−4.68	G74		−4.69	bad fit for the core
4	4481.150	−0.570	NIST	71490.19	−4.68	G74		−4.69	bad fit for the core
4	4481.325	+0.575	NIST	71490.06	−4.68	G74		−4.69	bad fit for the core
8	7877.054	+0.390	NIST	80619.50	−4.54	G74	64.50	−4.68	
8	7896.042	−0.303	NIST	80650.02	−4.54	G74	28.14	−4.77	
8	7896.366	+0.647	NIST	80650.02	−4.54	G74	85.58	−4.56	blend with telluric line
–	8213.987	−0.279	NIST	80619.50	−4.77	G74		−4.81	at the Paschen limit
–	8234.636	+0.024	NIST	80650.02	−4.77	G74		−4.81	blend with telluric line
–	9631.891	+0.663	NIST	93310.59	––	––	57.42	−4.69	
–	9631.95	−0.639	NIST	93310.59	––	––		−4.69	
–	9632.430	+0.507	NIST	93311.11	––	––	47.05	−4.72	
			Si II log N(Si II)/N$_{\rm tot}$=−4.72±0.08						
1	3853.665	−1.517	K,BBCB	55309.35	−4.91	G74	60.94	−4.77	
1	3856.018	−0.557	K,BBCB	55325.18	−4.91	G74	108.86	−4.81	
1	3862.595	−0.817	K,BBCB	55309.35	−4.91	G74	98.75	−4.71	
3.01	4072.709	−2.367	K,SG	79338.50	−4.51	LDA	1.95	−4.75	
3.01	4075.452	−1.403	K,SG	79355.02	−4.51	LDA	15.18	−4.72	
7.26	4190.724	−0.351	LA	108820.60	−5.07	LDA	7.52	−4.66	
7.26	4198.133	−0.611	LA	108778.70	−5.07	LDA	4.99	−4.59	
5	5041.024	+0.174	NIST	81191.34	−4.70	G74	73.40	−4.65	
5	5055.984	+0.441	NIST	81251.32	−4.70	G74	90.48	−4.65	
5	5056.317	−0.535	NIST	81251.32	−4.70	G74	38.52	−4.63	
7.03	5466.432	−0.190	NIST	101023.05	−3.85	G74	11.11	−4.74	
7.33	5669.563	+0.266	LA	114529.14	––	––	5.68	−4.75	
7.33	5688.817	+0.106	LA	114414.58	––	––	3.22	−4.87	
4	5957.559	−0.349	NIST	81191.34	−4.91	G74	37.52	−4.65	
4	5978.930	−0.061	NIST	81251.32	−4.91	G74	49.34	−4.65	
7.02	7848.816	+0.335	NIST	101023.05	−4.25	G74	11.81	−4.81	
7.02	7849.722	+0.492	NIST	101024.35	−4.25	G74	13.41	−4.89	
			Si III log N(Si III)/N$_{\rm tot}$=−4.58±0.04						
2	4552.622	+0.292	NIST	153377.05	––	––	4.01	−4.62	
2	4567.840	+0.069	NIST	153377.05	––	––	3.15	−4.54	

Table A.1. Abundances of the light elements, cont.

Mult.	λ(Å)	log gf	Ref.[a]	χ_{low}(cm^{-1})	γ_s	Ref.[b]	W(mÅ)	$log(N_Z/N_{\rm tot})$	Notes
		P II	log N(P II)/N$_{\rm tot}$=−6.28±0.08						
7	5296.077	−0.134	K,HI	87124.60	−−	−−	2.20	−6.33	
6	5316.055	−0.341	K,HI	86743.96	−4.09	G74	1.66	−6.28	
6	5344.729	−0.329	K,HI	86597.55	−4.09	G74	1.88	−6.24	
6	5386.895	−0.305	K,HI	86743.96	−4.09	G74	1.72	−6.29	
6	5425.880	+0.241	K,HI	87124.60	−4.09	G74	4.20	−6.39	
5	6024.178	+0.137	K,HI	87124.60	−4.40	G74	1.37	−6.20	
5	6034.039	−0.209	K,HI	86597.55	−4.40	G74	2.15	−6.15	
5	6043.084	+0.384	K,HI	87124.60	−4.40	G74	4.09	−6.41	
5	6034.039	−0.209	K,HI	86597.55	−4.40	G74	2.15		
		S II	log N(S II)/N$_{\rm tot}$=−5.12±0.03						
44	4153.068	+0.617	NIST	128233.20	−−	−−	8.25	−5.09	
44	4162.665	+0.777	NIST	128599.16	−−	−−	9.53	−5.13	
1	5027.203	−0.705	NIST	105599.06	−−	−−	3.05	−5.08	
1	5142.322	−0.822	NIST	106044.24	−−	−−	1.92	−5.13	
39	5212.620	+0.318	NIST	121530.02	−−	−−	3.64	−5.17	
6	5453.855	+0.482	NIST	110268.60	−−	−−	11.70	−5.10	
		Ca I	log N(Ca I)/N$_{\rm tot}$=−5.26						
2	4226.728	+0.244	NIST	0.00	−5.74	G74	2.4	−5.26	
		Ca II	log N(Ca II)/N$_{\rm tot}$=−5.67±0.25						
4	3158.869	+0.252	K,BWL	25191.51	−5.07	G74	46.4	−5.90	
4	3179.331	+0.512	K,BWL	25414.40	−5.07	G74	57.4	−5.76	
4	3181.275	−0.448	K,BWL	25414.40	−5.07	G74	29.7	−5.83	
3	3706.024	−0.447	K,BWL	25191.51	−5.09	G74		−5.54	wings of H_{15}, H_{16}
3	3736.902	−0.147	K,BWL	25414.40	−5.09	G74		−5.60	red wing of H_{13}
1	3933.664	+0.134	K,BWL	0.00	−5.52	G74		−5.54	bump on the red wing
1	3968.469	−0.179	K,BWL	0.00	−5.52	G74		−5.54	blue wing of H_ϵ, red component
15	5001.479	−0.517	K,BWL	60533.53	−4.24	G74		−5.64	blend with Fe II
15	5019.971	−0.257	K,BWL	60611.28	−4.24	G74		−5.64	blend with Fe II
15	5021.138	−1.217	K,BWL	60611.28	−4.24	G74		−5.54:	weak
14	5285.266	−1.153	K,BWL	60533.02	−4.30	G74		−5.54:	weak
14	5307.224	−0.853	K,BWL	60611.28	−4.30	G74		−−	blend with an unknown component
13	8201.720	+0.315	K,BWL	60533.02	−4.62	G74		−−	telluric line
13	8248.796	+0.572	NIST	60611.28	−4.62	G74		−6.40	at the Paschen limit
13	8254.721	−0.388	NIST	60611.28	−4.62	G74		−5.8??	weak, at the Paschen limit
2	8498.023	−1.312	K,BWL	13650.19	−5.55	G74		−5.54	shifted by +0.2 Å,blue wing of P_{15}
2	8542.091	−0.362	K,BWL	13710.88	−5.55	G74			no observations
2	8662.141	−0.623	K,BWL	13650.19	−5.55	G74		−5.20	shifted by +0.2 Å, blue wing of P_{13}
12	9854.759	−0.228	K,BWL	60533.02	−4.66	G74		≤−5.54	bad spectrum, low S/N
12	9931.374	+0.072	K,BWL	60611.28	−4.66	G74		≤−5.54	bad spectrum, low S/N

[a] "K" before another log gf source means that the log gf is from Kurucz files available at http://kurucz.harvard.edu/linelists/gf100
(BBCB) Berry et al. 1971; (BIE) Biémont 1977; (BWL) Black et al. 1972; (CNO) Wiese et al. 1996;
(HI) Hibbert 1988; (KP) Kurucz & Peytremann 1975; (LA) Lanz & Artru 1985; (NBS) Wiese et al. 1966; (NIST) http://physics.nist.gov/cgi-bin/AtData/lines_form; (SG) Schulz-Gulde 1969

[b] (BCS1) Barnard et al. 1974; (BCS2) Barnard et al. 1975; (DS90) Dimitrijevic & Sahal-Brechot 1990; (G74) Griem 1974; (LDA) Lanz et al. 1988; (SM69) Shamey 1969

Table A.2. Abundances of the iron group elements.

Mult.	λ(Å)	log gf	Ref.[a]	χ_{low}	W(mÅ)	$log(N_Z)/N_{\rm tot})$	Notes
			Sc II	logN(Sc II)/N$_{\rm tot}$=−9.08±0.15			
3	3580.925	−0.070	K,MFW	0.00	2.02	−8.89	
2	3613.829	+0.520	K,MFW	177.76	5.81	−8.96	
2	3630.742	+0.340	K,MFW	67.76	4.28	−8.94	
2	3642.784	+0.180	K,MFW	0.00	2.73	−8.99	
7	4246.822	+0.320	K,MFW	2540.95	4.44	−9.37	
15	4314.083	−0.100	K,MFW	4987.79	1.96	−9.17	
14	4374.457	−0.440	K,MFW	4987.79	1.07	−9.10	
31	5526.790	+0.130	K,MFW	14261.32	0.86	−9.19	
			Ti II	logN(Ti II)/N$_{\rm tot}$=−5.67 ±0.11			
5	3072.107	−0.620	PTP	225.73	61.34	−5.43	
4	3121.598	−2.360	PTP	0.00	16.36	−5.51	
4	3130.798	−1.190	PTP	94.10	44.49	−5.54	
10	3145.396	−2.600	PTP	983.89	7.31	−5.69	
4	3157.393	−2.170	PTP	94.10	18.33	−5.61	
10	3161.201	−0.690	PTP	908.02	54.92	−5.57	
10	3161.769	−0.550	PTP	983.89	59.71	−5.52	
10	3162.566	−0.380	PTP	1087.32	60.63	−5.65	
10	3168.518	−0.200	PTP	1215.84	66.26	−5.61	
3	3214.767	−1.400	PTP	393.44	38.79	−5.53	
2	3222.841	−0.420	PTP	94.10	63.99	−5.55	
3	3226.769	−1.840	PTP	225.73	26.00	−5.61	
2	3234.514	+0.430	PTP	393.44	86.84	−5.67	
23	3236.119	−0.430	PTP	8710.44	48.44	−5.53	
2	3236.572	+0.240	PTP	225.73	79.21	−5.70	
2	3239.036	+0.070	PTP	94.10	76.96	−5.60	
23	3239.661	−0.200	PTP	8744.25	76.96	−5.53	
2	3241.983	−0.030	PTP	0.00	76.81	−5.51	
23	3249.366	−1.360	PTP	8710.44	24.74	−5.57	
2	3251.908	−0.590	PTP	94.10	59.53	−5.55	
2	3254.245	−0.560	PTP	393.44	58.86	−5.58	
7	3308.803	−1.140	PTP	1087.32	41.01	−5.64	
7	3318.023	−1.040	PTP	983.89	46.15	−5.55	
7	3343.761	−1.150	PTP	1215.84	40.92	−5.63	
7	3346.741	−1.060	PTP	1087.42	45.59	−5.54	
1	3361.212	+0.430	PTP	225.73	84.33	−5.69	
1	3372.793	+0.280	PTP	94.10	79.51	−5.69	
1	3380.279	−0.570	K,MFW	393.44	61.97	−5.44	
1	3383.759	+0.160	PTP	0.00	87.01	−5.36	
6	3477.180	−0.960	PTP	983.89	46.13	−5.61	
6	3489.736	−1.980	PTP	1087.32	17.60	−5.71	
6	3500.330	−2.100	PTP	983.89	18.55	−5.56	
15	3561.575	−1.940	PTP	4268.58	11.65	−5.81	
15	3573.731	−1.490	PTP	4628.58	24.62	−5.66	
15	3587.131	−1.590	PTP	4897.65	22.00	−5.65	
15	3596.047	−1.030	PTP	4897.65	37.79	−5.58	
34	3900.539	−0.200	PTP	9118.26	76.60	−5.96	
34	3913.461	−0.420	PTP	8997.71	77.23	−5.73	
11	4012.383	−1.840	PTP	4628.58	41.10	−5.67	
87	4053.821	−1.130	PTP	15265.62	40.03	−5.76	
21	4161.529	−2.360	K,MFW	8744.25	17.44	−5.55	
105	4163.644	−0.130	PTP	20891.66	62.40	−5.77	
20	4287.873	−1.790	PTP	8710.44	27.82	−5.82	
41	4290.215	−0.850	PTP	9395.71	65.27	−5.71	
20	4294.094	−0.930	PTP	8744.25	63.27	−5.72	
41	4300.042	−0.440	PTP	9518.06	78.06	−5.74	
41	4301.922	−1.150	PTP	9363.62	54.33	−5.73	
41	4312.860	−1.100	PTP	9518.05	57.56	−5.68	
41	4314.971	−1.100	PTP	9363.62	55.37	−5.75	
41	4320.950	−1.800	PTP	9395.71	24.78	−5.85	

Table A.2. Abundances of the iron group elements, cont.

Mult.	λ(Å)	log gf	Ref.[a]	χ_{low}	W(mÅ)	$log(N_Z)/N_{\rm tot})$	Notes
			Ti II cont.				
104	4367.652	−0.860	PTP	20891.66	35.88	−5.80	
93	4374.816	−1.610	PTP	16625.11	21.38	−5.70	
104	4386.847	−0.960	PTP	20951.62	31.82	−5.80	
51	4394.059	−1.780	PTP	9850.90	30.58	−5.69	
19	4395.031	−0.540	PTP	8744.25	79.02	−5.64	
51	4399.765	−1.190	PTP	9975.92	54.35	−5.66	
115	4411.072	−0.670	PTP	24961.03	31.84	−5.84	
40	4417.714	−1.190	PTP	9395.71	55.39	−5.66	
51	4418.331	−1.970	PTP	9395.71	19.61	−5.80	
40	4441.729	−2.330	PTP	9518.06	11.70	−5.76	
19	4443.801	−0.720	PTP	8710.44	72.95	−5.65	
19	4450.482	−1.520	PTP	8744.25	42.66	−5.72	
40	4464.448	−1.810	PTP	9363.62	28.90	−5.74	
31	4468.492	−0.600	K,MFW	9118.26	75.93	−5.65	
115	4488.325	−0.510	PTP	25192.79	37.27	−5.84	
31	4501.270	−0.770	PTP	8997.71	71.44	−5.63	
50	4533.960	−0.530	PTP	9975.92	77.23	−5.64	
60	4544.016	−2.580	PTP	10024.73	6.49	−5.77	
50	4563.757	−0.690	PTP	9850.90	68.15	−5.76	
82	4571.971	−0.320	PTP	12676.97	81.77	−5.56	
59	4657.206	−2.240	PTP	10024.73	12.39	−5.79	
49	4708.662	−2.340	PTP	9975.92	10.08	−5.80	
92	4779.985	−1.370	K,MFW	16515.86	32.07	−5.65	
17	4798.532	−2.680	PTP	8710.44	7.48	−5.69	
92	4805.085	−1.100	K,MFW	16625.11	45.57	−5.57	
114	4911.195	−0.610	PTP	25192.79	36.40	−5.76	
113	5069.092	−1.820	PTP	25192.79	5.75	−5.66	
113	5072.287	−1.060	PTP	25192.79	20.15	−5.75	
—	5154.070	−1.750	PTP	12628.73	22.57	−5.77	
86	5185.902	−1.490	PTP	15265.62	32.05	−5.61	
—	5188.687	−1.050	PTP	12758.11	50.88	−5.72	
—	5226.538	−1.260	PTP	12628.73	44.34	−5.69	
103	5268.615	−1.620	K,MFW	20951.62	11.80	−5.76	
—	5336.786	−1.590	PTP	12758.11	29.32	−5.73	
—	5381.021	−1.920	PTP	12628.73	16.59	−5.78	
			Cr I log N(Cr I)/N$_{\rm tot}$ = −5.22±0.09				
4	3578.686	+0.409	K,MFW	0.00	6.26	−5.17	
4	3593.485	+0.307	K,MFW	0.00	4.52	−5.24	
4	3605.329	+0.197	K,MFW	0.00	4.41	−5.14	
1	4254.336	−0.114	K,MFW	0.00	6.40	−5.27	
1	4274.797	−0.231	K,MFW	0.00	4.23	−5.35	
1	4289.717	−0.361	K,MFW	0.00	3.28	−5.34	
7	5204.511	−0.208	K,MFW	7593.15	2.54	−5.16	
7	5206.037	+0.019	K,MFW	7593.15	4.93	−5.08	
7	5208.425	+0.158	K,MFW	7593.15	4.62	−5.25	
			Cr II log N(Cr II)/N$_{\rm tot}$ = −5.41 ±0.07				
5	3118.646	−0.000	K,MFW	19528.25	74.61	−5.38	
5	3120.359	+0.120	K,MFW	19631.17	78.48	−5.38	
54	3122.596	−0.110	K,MFW	33694.15	49.42	−5.25	
39	4539.595	−2.280	SL	32603.40	13.96	−5.42	
44	4558.650	−0.410	SL	32854.31	79.21	−5.34	
39	4565.770	−1.860	SL	32603.40	27.00	−5.43	
—	4587.264	−1.648	K,MFW	52321.01	3.77	−5.53	
44	4588.199	−0.643	K,MFW	32836.68	71.39	−5.35	
44	4592.049	−1.217	K,MFW	32854.95	44.53	−5.58	
44	4616.629	−1.291	K,MFW	32844.76	44.28	−5.51	
44	4618.803	−0.860	SL	32854.95	64.13	−5.35	
44	4634.070	−0.990	SL	32844.76	57.91	−5.41	

Table A.2. Abundances of the iron group elements, cont.

Mult.	λ(Å)	log gf	Ref.[a]	χ_{low}	W(mÅ)	$log(N_Z)/N_{\rm tot})$	Notes
			Cr II cont.				
−−	4697.598	−1.882	K,MFW	45730.58	6.36	−5.44	
30	4812.337	−1.995	K,K88	31168.58	24.44	−5.44	
30	4824.127	−0.970	SL	31219.35	65.81	−5.28	
30	4836.229	−2.000	SL	31117.39	25.57	−5.38	
43	5237.329	−1.160	K,MFW	32854.31	53.12	−5.38	
23	5246.768	−2.450	K,MFW	29951.88	14.55	−5.39	
43	5279.880	−2.100	K,MFW	32854.31	21.07	−5.33	
24	5305.860	−2.080	K,MFW	30864.76	24.27	−5.38	
43	5308.440	−1.810	K,MFW	32836.68	24.04	−5.53	
43	5310.700	−2.280	K,MFW	32844.76	14.54	−5.38	
43	5313.590	−1.650	K,MFW	32854.95	34.42	−5.40	
23	5420.922	−2.360	K,MFW	30307.44	13.80	−5.48	
50	5502.067	−1.990	K,MFW	33618.94	20.73	−5.40	
50	5508.606	−2.110	K,MFW	33521.11	16.35	−5.43	
105	6053.466	−2.160	K,MFW	38269.59	8.21	−5.44	
		Mn I log N(Mn I)/$N_{\rm tot}$=−4.20±0.08					
8	3577.868	+0.160	K,MFW	17052.29	6.54	−4.29	
8	3595.107	−0.860	K,MFW	17451.52	0.75	−4.27	
8	3607.526	−0.440	K,MFW	17282.00	2.21	−4.21	
8	3608.481	−0.370	K,MFW	17451.52	3.18	−4.09	
5	4018.100	−0.309	K,MFW	17052.29	12.27	−4.18	
2	4030.753	−0.470	K,MFW	0.00	40.68	−4.18	(W,log(N/$N_{\rm tot}$)$_{JDA}$)=(41.0,−4.35)[b]
2	4034.483	−0.811	K,MFW	0.00	23.85	−4.32	(W,log(N/$N_{\rm tot}$)$_{JDA}$)=(23.0,−4.50)[b]
5	4041.355	+0.258	K,MFW	17052.29	36.24	−4.02	
5	4055.544	−0.070	K,MFW	17282.00	17.59	−4.20	
5	4070.278	−0.950	K,MFW	17637.15	2.81	−4.22	
5	4082.939	−0.354	K,MFW	17568.48	10.33	−4.20	
22	4453.012	−0.490	K,MFW	23719.52	3.39	−4.24	
28	4457.044	−0.555	K,MFW	24788.05	1.66	−4.43	
28	4458.254	+0.042	K,MFW	24788.05	7.42	−4.33	
28	4461.079	−0.380	K,MFW	24802.25	4.22	−4.18	
28	4462.031	+0.320	K,MFW	24802.25	14.74	−4.25	
22	4464.682	−0.104	K,MFW	23549.20	6.79	−4.31	
−−	4479.393	+0.010	K,MFW	41230.30	1.74	−3.99	
22	4490.080	−0.522	K,MFW	23818.87	3.30	−4.21	
22	4502.213	−0.345	K,MFW	23549.20	4.60	−4.26	
−−	4626.530	+0.210	K,MFW	38008.70	4.76	−3.92	
21	4727.461	−0.470	K,MFW	23549.20	3.96	−4.20	
21	4739.110	−0.490	K,MFW	23719.52	3.46	−4.23	
21	4762.367	+0.425	K,MFW	23296.67	20.45	−4.24	
21	4765.846	−0.080	K,MFW	23719.52	9.77	−4.14	
21	4766.418	+0.100	K,MFW	23549.20	13.73	−4.14	
16	4783.427	+0.042	K,MFW	18531.64	21.56	−4.12	
16	4823.524	+0.144	K,MFW	18705.37	23.71	−4.14	
27	6013.480	−0.251	K,MFW	25779.32	5.92	−4.13	
27	6021.790	+0.034	K,MFW	24802.25	9.24	−4.19	
		Mn II log N(Mn II)/$N_{\rm tot}$=−4.25±0.04					
3	3441.988	−0.272	K,MFW	14325.86	176.9	−4.27	
3	3460.316	−0.542	K,MFW	14593.82	140.3	−4.25	
3	3482.905	−0.740	K,MFW	14781.19	117.2	−4.28	
3	3488.677	−0.864	K,MFW	14910.18	108.8	−4.26	
3	3495.833	−1.218	K,MFW	14959.84	92.87	−4.15	
3	3496.809	−1.687	K,MFW	14781.19	69.99	−4.27	
3	3497.526	−1.330	K,MFW	14901.18	82.89	−4.26	
		The Mn II lines used by Jomaron et al. (1999) (JDA)					
−−	3917.318	−1.147	K,K88	55759.27	39.59	−4.55	(W,log(N/$N_{\rm tot}$)$_{JDA}$)=(43.5,−4.52)[b]
−−	4363.258	−1.909	K,K88	44899.82	39.35	−4.43	(W,log(N/$N_{\rm tot}$)$_{JDA}$)=(37.5,−4.54)[b]
−−	4365.219	−1.350	K,K88	53017.16	40.60	−4.46	(W,log(N/$N_{\rm tot}$)$_{JDA}$)=(40.5,−4.59)[b]
−−	4478.635	−0.950	K,K88	53597.13	54.37	−4.39	(W,log(N/$N_{\rm tot}$)$_{JDA}$)=(55.0,−4.66)[b]

Table A.2. Abundances of the iron group elements, cont.

Mult.	λ(Å)	log gf	Ref.[a]	χ_{low}	W(mÅ)	$log(N_Z)/N_{\rm tot})$	Notes
			Fe I log N(Fe I)/$N_{\rm tot}$ = −4.78±0.08				
23	3581.193	+0.406	K,FMW	6928.27	6.90	−4.84	
23	3618.768	+0.000	K,FMW	7985.78	2.06	−4.97	
43	4005.242	−0.610	K,FMW	12560.93	1.96	−4.75	
43	4045.812	+0.280	K,FMW	11976.24	12.67	−4.78	
43	4071.738	−0.022	K,FMW	12698.55	6.26	−4.78	
42	4202.029	−0.708	K,FMW	11976.24	1.94	−4.70	
419	4219.360	+0.120	K,FMW	28819.95	1.02	−4.81	
152	4235.936	−0.341	K,FMW	19562.44	1.12	−4.86	
42	4271.760	−0.164	K,FMW	11976.24	6.74	−4.67	
41	4383.545	+0.200	K,FMW	11976.24	12.06	−4.74	
41	4404.750	−0.142	K,FMW	12560.93	6.09	−4.71	
41	4415.122	−0.615	K,FMW	12968.55	2.00	−4.72	
			Fe II log N(Fe II)/$N_{\rm tot}$ = −4.84±0.13				
173	3906.035	−1.830	K,FMW	44929.55	15.01	−4.80	
3	3914.503	−4.050	K,FMW	13473.41	4.38	−5.04	
173	3935.962	−1.860	K,FMW	44915.05	16.00	−4.73	
3	3938.290	−3.890	K,FMW	13471.41	8.55	−4.88	
3	3945.210	−4.250	K,FMW	13673.18	3.84	−4.89	
28	4122.668	−3.380	K,FMW	20830.58	10.98	−4.83	
27	4128.748	−3.770	K,FMW	20830.58	6.90	−4.67	
28	4178.862	−2.480	K,FMW	20830.58	34.36	−4.96	
28	4258.154	−3.400	K,FMW	21812.05	7.57	−4.94	
27	4273.326	−3.258	K,FMW	21812.05	10.74	−4.90	
28	4296.572	−3.010	K,FMW	21812.05	19.75	−4.80	
27	4303.176	−2.490	K,FMW	21812.05	34.78	−4.88	
28	4369.411	−3.670	K,FMW	22409.85	5.04	−4.83	
27	4385.387	−2.570	K,FMW	22409.85	24.50	−5.06	
32	4413.601	−3.870	K,FMW	21581.64	2.06	−5.09	
27	4416.830	−2.600	K,FMW	22409.85	30.13	−4.86	
37	4491.405	−2.700	K,FMW	23031.30	24.60	−4.88	
38	4508.288	−2.210	K,FMW	23031.30	37.25	−5.01	
37	4515.339	−2.480	K,FMW	23939.36	31.54	−4.85	
37	4520.224	−2.600	K,FMW	22637.21	29.09	−4.88	
38	4522.634	−2.030	K,FMW	22939.36	44.78	−4.98	
38	4541.524	−3.050	K,FMW	23031.30	17.41	−4.76	
186	4549.192	−1.870	K,FMW	47674.72	15.09	−4.57	
38	4549.474	−1.750	K,FMW	22810.36	53.65	−5.01	
37	4555.893	−2.290	K,FMW	22810.36	34.65	−5.02	
38	4576.340	−3.040	K,FMW	22939.36	18.15	−4.75	
37	4582.835	−3.100	K,FMW	22939.36	12.89	−4.89	
38	4583.837	−2.020	K,FMW	22637.21	55.43	−4.69	
38	4620.521	−3.280	K,FMW	22810.36	10.08	−4.85	
186	4635.316	−1.650	K,FMW	47674.72	18.70	−4.65	
43	4656.981	−3.630	K,FMW	23317.63	5.90	−4.74	
37	4666.758	−3.330	K,FMW	22810.36	9.50	−4.83	
25	4670.182	−4.100	K,FMW	20830.58	2.12	−4.89	
43	4731.453	−3.360	K,FMW	23317.63	13.19	−4.59	
42	4923.927	−1.320	K,FMW	23317.63	75.84	−4.73	
36	4993.358	−3.650	K,FMW	22637.20	4.71	−4.86	
42	5018.440	−1.220	K,FMW	23317.63	83.50	−4.64	
35	5132.669	−4.180	K,FMW	22637.20	2.35	−4.65	
42	5169.033	−0.870	K,FMW	23317.63	88.23	−4.86	
49	5197.577	−2.100	K,FMW	26055.42	36.50	−4.93	
49	5234.625	−2.050	K,FMW	25981.63	37.62	−4.95	
−−	5247.952	+0.630	K,FMW	84938.18	11.82	−5.02	

Table A.2. Abundances of the iron group elements, cont.

Mult.	λ(Å)	log gf	Ref.[a]	χ_{low}	W(mÅ)	$log(N_Z)/N_{tot}$)	Notes
			Fe II cont.				
185	5272.397	−2.030	K,FMW	48039.09	9.61	−4.60	
49	5276.002	−1.940	K,FMW	25805.33	39.99	−5.00	
41	5284.109	−3.190	K,FMW	23317.63	13.28	−4.74	
49	5316.615	−1.850	K,FMW	25428.78	47.28	−4.90	
49	5425.257	−3.360	K,FMW	25805.33	3.74	−5.05	
−−	5506.195	+0.950	K,FMW	84863.35	21.48	−4.90	
55	5534.847	−2.930	K,FMW	26170.18	16.85	−4.68	
−−	5961.705	+0.699	K,FMW	86124.30	13.10	−4.88	
46	6084.110	−3.980	K,FMW	25805.33	1.95	−4.70	
74	6149.258	−2.724	K,K88	31368.45	10.38	−4.81	
−−	6383.722	−2.271	K,FMW	44784.76	3.01	−5.05	
74	6416.919	−2.850	K,FMW	31387.95	8.55	−4.78	
74	6456.383	−2.300	K,FMW	31483.176	25.58	−4.64	
			Ni II	$\log N(\mathrm{Ni\,II})/N_{tot} = -6.09 \pm 0.16$			
1	3274.916	−2.805	K03	23108.28	2.20	−6.03	
5	3290.534	−2.755	K03	25036.38	1.67	−6.08	
1	3290.683	−3.016	K03	23796.18	2.28	−5.76	
1	3350.419	−2.355	K03	23796.18	5.77	−5.94	
1	3373.969	−2.006	K03	23108.28	10.27	−5.99	
4	3401.766	−2.682	K03	24788.20	1.58	−6.17	
4	3407.300	−1.855	K03	24835.93	9.51	−6.07	
1	3454.164	−2.146	K03	23796.18	6.73	−6.04	
4	3471.386	−1.902	K03	24835.93	8.71	−6.06	
1	3513.987	−1.507	K03	23108.28	19.35	−5.97	
4	3576.764	−1.676	K03	24788.20	11.65	−6.08	
12	4015.474	−2.410	K03	32523.54	3.79	−6.35	
11	4067.031	−1.834	K03	32499.53	10.74	−6.41	
10	4192.065	−3.270	K03	32523.54	1.12	−6.04	
9	4244.779	−3.095	K03	32523.54	0.89	−6.31	

[a] "K" before another log gf source means that the log gf is from Kurucz files available at http://kurucz.harvard.edu/linelists/gf100 (FMW) Fuhr et al. 1988; (K88) Kurucz 1988; (K03) Kurucz 2003; (MFW) Martin et al. 1988; (PTP) Pickering et al. 2002; (SL) Sigut & Landstreet 1990

[b] Equivalent widths W and abundances from Jomaron, Dworetsky & Allen (1999) (JDA)

Table A.3. Abundances of elements with Z≥31.

mult	λ(Å)	log gf	Ref.[a]	χ_{low}(cm^{-1})	χ_{up}(cm^{-1})	W(mÅ)	log N/N$_{tot}$	Notes
		Ga II	log N(Ga II)/N$_{tot}$=−5.43±0.04					
−−	4251.149	+0.35	RS94	113815.92	137332.35		−5.20	
−−	4254.075	−0.23	RS94	113842.19	137342.44		−5.20	
−−	4255.722	+0.634	NKW,RS94	113842.19	137333.33		−5.45	bad fit, missing components
−−	4255.937	−0.32	NKW,RS94	113842.19	137332.35		−5.45:	blend with (wrong?) Mn II
−−	4262.014	+0.98	RS94	113883.19	137339.64		−5.45	blend with Cr II+Cr II
−−	5338.240	+0.43	RS94	118430.20	137157.48		−5.65:	bad fit
−−	5360.402	+0.42	RS94	118518.47	137168.47		−5.45	
−−	5363.585	+0.06	NKW	118518.47	137157.48		−5.45	blend with (wrong?) Cr II
−−	5416.318	+0.64	RS94	118727.89	137185.30		−5.25	
−−	5421.275	−0.05	NKW	118727.89	137168.47		−5.45	
−−	6334.069	+1.00	RS94	102944.55	118727.89		−5.65	
−−	6419.239	+0.57	RS94	102944.55	118518.47		−5.55	blend with (wrong?) Cr II
−−	6455.923	−0.08	RS94	102944.55	118430.02		−5.45	blend with O I
		guessed log gfs for Ga II						
−−	4261.478	−1.10	GUESS	113883.19	137342.44			
−−	4263.136	−0.50	GUESS	113883.19	137333.33			
−−	5219.658	+0.35	GUESS	120550.27	139703.28			
−−	7198.450	+0.25	GUESS	106662.21	120550.27			
−−	7792.260	+0.00	GUESS	107720.56	120550.27			
		Br II	log N(Br II)/N$_{tot}$=−7.12±0.04					
−−	4704.850	+0.408	NIST	93921.34	115176.00	1.09	−7.16	
−−	4785.500	+0.208	NIST	93921.54	114818.00	0.85	−7.07	
		Sr II	log N(Sr II)/N$_{tot}$=−8.41					
1	4077.709	+0.151	NIST	0.00	24516.65	26.66	−8.41	
		Y II	log N(Y II)/N$_{tot}$=−6.66±0.20					
10	3195.616	−0.420	K,HL	840.21	32124.04	28.64	−6.35	
10	3200.272	−0.430	K,HL	1045.08	32283.40	26.37	−6.45	
10	3203.322	−0.370	K,HL	840.21	32048.78	27.86	−6.44	
10	3216.682	−0.020	K,HL	1045.08	32124.04	35.67	−6.35	
10	3242.280	+0.210	K,HL	1449.81	32283.40	40.16	−6.32	
18	3327.878	+0.130	K,CC	3296.18	33336.72	32.32	−6.51	
3	3496.081	−0.720	K,HL	0.00	28595.27	20.64	−6.48	
9	3549.005	−0.280	K,HL	1045.08	29213.95	27.34	−6.48	
9	3584.514	−0.410	K,HL	840.21	28730.01	24.78	−6.49	
9	3600.741	+0.280	K,HL	1044.81	29213.95	42.41	−6.24	
9	3601.919	−0.180	K,HL	840.21	28595.27	32.75	−6.30	
9	3611.044	+0.110	K,HL	1045.08	28730.07	33.79	−6.52	
2	3633.122	−0.100	K,HL	1045.08	27516.69	30.44	−6.54	
7	3818.341	−0.980	K,HL	1045.08	27227.04	23.35	−6.90	
16	3930.660	−1.610	K,HL	3296.18	28730.01	8.63	−6.76	
6	3950.352	−0.490	K,HL	840.21	26147.25	39.01	−6.84	
16	3951.593	−1.980	K,HL	3296.18	28595.27	3.22	−6.88	
6	3982.594	−0.490	K,HL	1045.08	26147.25	36.23	−6.94	
5	4199.277	−2.150	K,HL	840.21	24647.13	3.55	−6.82	
1	4204.695	−1.760	K,HL	0.00	23776.24	7.89	−6.87	
5	4235.729	−1.500	K,HL	1045.08	24647.13	10.66	−6.91	
5	4309.631	−0.750	K,HL	1449.81	24647.13	30.09	−6.89	
5	4358.728	−1.329	K,HL	840.21	23776.24	14.58	−6.91	
22	4883.684	+0.070	K,HL	8743.32	29213.94	46.51	−6.64	
22	4900.120	−0.090	K,HL	8328.04	28730.01	42.70	−6.66	
20	4982.129	−1.290	K,HL	8328.04	28394.18	7.22	−6.88	
20	5087.416	−0.170	K,HL	8743.32	28394.18	38.33	−6.72	
20	5119.112	−1.360	K,HL	8003.12	27532.32	7.41	−6.82	

Table A.3. Abundances of elements with Z≥31, cont.

Mult.	λ(Å)	log gf	Ref.[a]	χ_{low}(cm^{-1})	χ_{up}(cm^{-1})	W(mÅ)	$log(N_Z)/N_{\rm tot}$)	Notes
			Y II cont.					
20	5200.406	−0.570	K,HL	8003.12	27227.04	25.20	−6.83	
20	5205.724	−0.342	K,HL	8328.04	27532.32	35.39	−6.68	
27	5473.388	−1.020	K,HL	14081.26	32283.40	7.68	−6.76	
27	5480.732	−0.990	K,HL	13833.38	32124.04	7.38	−6.82	
27	5497.408	−0.580	K,HL	14098.07	32283.40	18.31	−6.68	
27	5546.009	−1.100	K,HL	14098.07	32124.04	7.44	−6.69	
38	5662.925	+0.160	K,CC	15682.90	33336.72	40.07	−6.51	
34	5728.890	−1.120	K,HL	14832.85	32283.40	5.61	−6.76	
32	7881.881	−0.572	K,HL	14832.85	27516.69	11.95	−6.82	
			Zr II log N(Zr II)/N$_{\rm tot}$=−8.67±0.17					
3	3279.266	−0.230	K,CC'	736.44	31249.28	2.47	−8.35	
1	3391.982	+0.463	K,CC'	1322.91	30795.74	5.15	−8.63	
46	3479.383	+0.170	K,BG	5752.92	34485.42	1.00	−8.83	
10	3496.192	+0.189	K,CC	314.67	28909.04	2.60	−8.78	
41	4149.217	−0.030	K,CC	6467.61	30561.75	2.34	−8.78	
			Rh II log N(Rh II)/N$_{\rm tot}$=−8.50:					
1	3162.284	+0.000	K,GUESS	28834.60	60448.40			
5	3187.875	+0.000	K,GUESS	27801.40	59161.50			
1	3207.285	+0.000	K,GUESS	25376.90	56547.30			
2	3233.314	+0.000	K,GUESS	27439.40	58358.50			
6	3267.480	+0.000	K,GUESS	31730.50	62326.10			
5	3307.348	+0.000	K,GUESS	28131.40	58358.50			
4	3477.823 ?	+0.000	K,GUESS	27801.40	56547.30			
			Pd I log N(Pd I)/N$_{\rm tot}$=−6.41±0.30					
3	3242.700	−0.070	K,BG	6564.11	37393.71	3.63	−5.96	
2	3404.579	+0.320	K,BG	6564.11	35927.89	2.67	−6.47	
9	3553.080	+0.540	K,CB	11721.77	39858.33	0.82	−6.89	
2	3609.547	+0.050	K,BG	7754.40	35451.40	1.39	−6.40	
1	3634.690	+0.090	K,CB	6564.11	34068.93	2.02	−6.33	
			Xe II log N(Xe II)/N$_{\rm tot}$=−5.96±0.20					
−−	4603.01	0.018	WM80	95064.00	116783.00	3.62	−6.32	
−−	4844.33	0.491	WM80	93068.00	113705.00	11.33	−6.04	
−−	5292.22	0.351	WM80	93068.00	111959.00	10.80	−5.81	
−−	5372.39	−0.211	WM80	95064.00	113673.00	3.12	−5.96	
−−	5419.15	0.215	WM80	95064.00	113512.00	7.75	−5.80	
−−	5719.60	−0.746	WM80	96033.00	113512.00	1.79	−5.58	
−−	5976.46	−0.222	WM80	95054.00	111782.00	1.60	−6.12	
−−	6051.15	−0.252	WM80	95438.00	111959.00	1.46	−6.12	
−−	6097.59	−0.237	WM80	95397.00	111792.00	1.94	−5.99	
−−	6990.88	+0.200	WM80	99405.00	113705.00	2.52	−5.86	λ_{obs}=6990.82 Å
			Other identified weak Xe II lines					
−−	5260.44	−0.437	WM80	104250.00	123255.00			
−−	5261.95	+0.150	WM80	112925.00	131924.00			
−−	5438.96	−0.183	WM80	102799.00	121180.00			
−−	5472.61	−0.449	WM80	95437.00	113705.00			blend Cr II
−−	5531.07	−0.616	WM80	95437.00	113512.00			
−−	6036.20	−0.609	WM80	95397.00	111959.00			

Table A.3. Abundances of elements with Z≥31, cont.

Mult.	λ(Å)	log gf	Ref.[a]	χ_{low}(cm^{-1})	χ_{up}(cm^{-1})	W(mÅ)	$log(N_Z)/N_{\rm tot}$)	Notes
identified Xe II lines with no available log gf								
−−	4448.13	0.00	GUESS	123112.54	145587.61			
−−	4921.48	0.00	GUESS	102799.07	123112.54			
−−	5339.33	0.00	GUESS	93068.44	111792.17			
−−	5368.07	0.00	GUESS	105947.55	124571.09			
−−	5525.53	0.00	GUESS	124289.45	142382.13			
−−	5667.56	0.00	GUESS	96033.48	113679.89			
Ba II	log N(Ba II)/N$_{\rm tot}$=−9.27							
−−	4554.029	+0.163	K,NBS	0.00	21952.42		−9.27	
−−	4934.076	−0.150	K,NBS	0.00	20261.56	1.041	−9.35	
Pr III	log N(Pr III)/N$_{\rm tot}$=−9.62							
−−	5299.969	−0.530	DREAM	2893.14	21755.84		−9.62	
Nd III	log N(Nd III)/N$_{\rm tot}$=−9.57±0.08							
−−	5127.044	−1.080	DREAM	2388.00	21887.00	1.08	−9.50	
−−	5203.924	−1.190	DREAM	0.00	19211.00	0.82	−9.65	
Yb II	log N(Yb II)/N$_{\rm tot}$=−8.10±0.19							
−−	3478.834	+0.460	DREAM	30224.33	58961.37	3.457	−7.82	
−−	4180.810	−0.290	DREAM	30392.23	54304.30	1.064	−8.33	
−−	5335.159	−0.260	DREAM	30562.79	49301.16	1.865	−8.08	
−−	5352.954	−0.340	DREAM	30224.33	48900.41	1.280	−8.19	
Yb III	log N(Yb III)/N$_{\rm tot}$=−7.31±0.01							
−−	3325.514	−1.35	DREAM	42425.00	72487.00	3.24	−7.31	
−−	3384.013	−0.58	DREAM	53365.00	82907.00	3.63	−7.32	
Pt II	log N(Pt II)/N$_{\rm tot}$=−7.63							
−−	4514.124	−1.48	DSJ	29261.97	51408.37		−7.63	
Au II	log N(Au II)/N$_{\rm tot}$=−7.51±0.06							
−−	4016.672	−1.88	RW	48510.89	73403.84	1.06	−7.58	
−−	4052.790	−1.69	RW	48510.89	73178.29	2.09	−7.45	
Hg I	log N(Hg I)/N$_{\rm tot}$=−6.19±0.18							
−−	4046.599	−0.818	BLD	37645.08	62350.46	0.89	−6.37	
−−	5460.731	−0.185	BLD	44042.98	62350.46	3.05	−6.01	
Hg II	log N(Hg II)/N$_{\rm tot}$=−6.53±0.23							
−−	3983.890	−1.520	PS,SR	35514.00	60608.00		−6.30	
−−	6149.470	+0.150	SR	95714.41	111971.46	1.95	−6.58	

[a] "K" before another log gf source means that the log gf is from Kurucz files available at http://kurucz.harvard.edu/linelists/gf100
(BLD) Benck et al. 1989; (BG) Biémont et al. 1981; (CB) Corliss & Bozman 1962; (CC) Cowley & Corliss 1983; (CC') Cowley & Corliss 1983, out the fitting range; (DJS) Dworetsky et al. (1984); (DREAM) Biémont et al. 1999, http://www.umh.ac.be/ astro/dream.shtml; (GUESS) guessed values; (HL) Hannaford et al. 1982; (NBS) Miles & Wiese 1969; (NIST) http://physics.nist.gov/cgi-bin/AtData/lines_form; (NKW) Nielsen et al. 2000; (PS) Proffitt et al. 1999; (SR) Sansonetti & Reader 2001; (RS94) Ryabchikova & Smirnov 1994; (RW) Rosberg & Wyart 1997; (WM80) Wiese & Martin 1980

Table A.4. The Ti II emission lines. The line data are from Kurucz & Bell (1995).

λ_{calc}(Å)	Elem	log gf	E_{low}(cm^{-1})	conf	E_{up}(cm^{-1})	conf.	R_c(obs)	R_c(calc)	Notes[a]
5846.579	Ti II	−0.689	64979.150	(3F)4d e4G	82078.430	(3F)4f 4G	1.006	0.993	
5921.937	Ti II	−0.024	64979.150	(3F)4d e4G	81860.840	(3F)4f 4G	1.013	0.971	
5928.521	Ti II	−0.045	64979.150	(3F)4d e4G	81842.090	(3F)4f 2G	1.005	0.973	
5929.696	Ti II	+0.376	65243.460	(3F)4d e4G	82103.060	(3F)4f 4G	1.006	0.936	
5937.320	Ti II	−0.061	65446.270	(3F)4d e4H	82284.220	(3F)4f 2I	1.000	0.975	
5937.412	Ti II	+0.152	64886.480	(3F)4d e4G	81724.170	(3F)4f 4G	1.008	0.958	
5940.344	Ti II	+0.464	65243.460	(3F)4d e4G	82072.840	(3F)4f 4H	1.007	0.924	
5940.764	Ti II	−0.004	65095.800	(3F)4d e4G	81923.990	(3F)4f 2H	1.011	0.971	
5944.674	Ti II	−0.591	65095.800	(3F)4d e4G	81912.920	(3F)4f 4F	1.006	0.992	
5961.332	Ti II	−0.317	65308.300	(3F)4d e4H	82086.430	(3F)4f 4G	1.009	0.986	
5965.298	Ti II	−0.220	64979.150	(3F)4d e4G	81738.130	(3F)4f 4I	1.009	0.982	
5969.800	Ti II	−0.529	65274.600	(3F)4d 4D	82020.940	(3F)4f 4D	1.005	0.991	
5969.818	Ti II	−0.534	65095.800	(3F)4d e4G	81842.090	(3F)4f 2G	1.005	0.991	
5971.648	Ti II	+0.634	64866.480	(3F)4d e4G	81627.640	(3F)4f 4H	1.037	0.893	
5979.141	Ti II	−0.326	65598.730	(3F)4d 4D	82318.910	(3F)4f 2D	1.016	0.987	?
5983.979	Ti II	−0.182	64979.150	(3F)4d e4G	81685.810	(3F)4f 2G	1.000	0.979	
5987.388	Ti II	+0.673	64979.150	(3F)4d e4G	81676.300	(3F)4f 4H	1.046	0.886	
5988.980	Ti II	+0.012	65308.300	(3F)4d e4H	82001.010	(3F)4f 2I	1.016	0.971	
5989.486	Ti II	−0.205	65460.010	(3F)4d f2F	82151.310	(3F)4f 2F	1.004	0.982	
5990.839	Ti II	−0.105	65460.010	(3F)4d f2F	82147.540	(3F)4f 4F	1.002	0.978	
5994.938	Ti II	+0.808	65243.460	(3F)4d e4G	81919.580	(3F)4f 4I	1.013	0.861	
5995.668	Ti II	−0.348	65186.750	(3F)4d e4H	81860.840	(3F)4f 4G	1.000	0.987	
5995.708	Ti II	+0.184	65460.010	(3F)4d f2F	82133.990	(3F)4f 4D	1.000	0.959	
6001.395	Ti II	+0.751	65095.800	(3F)4d e4G	81753.980	(3F)4f 4H	1.051	0.872	
6001.895	Ti II	+0.193	65446.270	(3F)4d e4H	82103.060	(3F)4f 4G	1.004	0.959	
6002.418	Ti II	+0.280	65186.750	(3F)4d e4H	81842.090	(3F)4f 2G	1.022	0.948	
6005.194	Ti II	−0.202	65598.730	(3F)4d 4D	82246.370	(3F)4f 4D	1.000	0.983	
6005.786	Ti II	−0.217	65243.460	(3F)4d e4G	81889.460	(3F)4f 4I	1.000	0.983	
6012.750	Ti II	+1.103	65590.190	(3F)4d e4H	82216.910	(3F)4f 4I	0.995	0.792	
6012.804	Ti II	+0.743	65446.270	(3F)4d e4H	82072.840	(3F)4f 4H	0.993	0.879	
6015.753	Ti II	−0.040	65460.010	(3F)4d f2F	82078.430	(3F)4f 4G	1.000	0.975	
6022.697	Ti II	−0.367	65397.570	(3F)4d 4D	81966.830	(3F)4f 4P	1.000	0.988	
6024.933	Ti II*	−0.091	65274.600	(3F)4d 4D	81867.700	(3F)4f 4P	1.015	0.977	
6024.940	Ti II*	+0.152	65213.800	(3F)4d 4D	81806.880	(3F)4f 4F	1.015	0.961	
6029.271	Ti II	+0.670	65308.300	(3F)4d e4H	81889.460	(3F)4f 4I	1.053	0.892	
6039.682	Ti II	+0.264	65598.730	(3F)4d 4D	82151.310	(3F)4f 2F	1.012	0.953	
6040.120	Ti II	+0.650	65186.750	(3F)4d e4H	81738.130	(3F)4f 4I	1.036	0.896	
6041.058	Ti II	+0.288	65598.730	(3F)4d 4D	82147.540	(3F)4f 4F	1.000	0.951	
6042.201	Ti II	+0.169	65397.570	(3F)4d 4D	81943.250	(3F)4f 2F	1.035	0.961	
6046.008	Ti II	−0.278	65598.730	(3F)4d 4D	82133.990	(3F)4f 4D	1.021	0.986	
6046.546	Ti II	+0.126	65308.300	(3F)4d e4H	81842.090	(3F)4f 2G	1.000	0.964	
6053.297	Ti II	+0.169	65397.570	(3F)4d 4D	81912.920	(3F)4f 4F	1.014	0.961	
6059.156	Ti II	+0.143	65274.600	(3F)4d 4D	81773.980	(3F)4f 4F	1.024	0.963	
6065.306	Ti II	+0.379	65590.190	(3F)4d e4H	82072.840	(3F)4f 4H	1.000	0.941	
6066.392	Ti II	+0.121	65598.730	(3F)4d 4D	82078.430	(3F)4f 4G	1.024	0.966	
6068.745	Ti II	+0.558	65446.270	(3F)4d e4H	81919.580	(3F)4f 4I	1.000	0.915	
6072.446	Ti II	+0.141	65397.570	(3F)4d 4D	81860.840	(3F)4f 4G	1.009	0.963	
6073.760	Ti II	−0.139	65314.270	(3F)4d f2F	81773.980	(3F)4f 4F	1.022	0.980	
6076.270	Ti II	−0.037	65460.010	(3F)4d 4D	81724.170	(3F)4f 4G	1.008	0.975	
6078.941	Ti II	+0.206	65308.300	(3F)4d e4H	81753.980	(3F)4f 4H	1.011	0.958	
6079.862	Ti II	−0.009	65446.270	(3F)4d e4H	81889.460	(3F)4f 4I	1.007	0.974	
6080.712	Ti II	+0.003	65186.750	(3F)4d e4H	81627.640	(3F)4f 4H	1.000	0.972	
6102.542	Ti II	+0.178	65460.010	(3F)4d f2F	81842.090	(3F)4f 2G	1.011	0.961	
6106.471	Ti II	+0.416	65314.270	(3F)4d f2F	81685.810	(3F)4f 2G	1.042	0.936	
6107.791	Ti II	−0.371	65308.300	(3F)4d e4H	81676.300	(3F)4f 4H	1.004	0.988	
6123.782	Ti II	−0.325	65598.730	(3F)4d 4D	81923.990	(3F)4f 2H	1.006	0.987	
6128.245	Ti II	−0.629	65314.270	(3F)4d f2F	81627.640	(3F)4f 4H	1.008	0.993	

Table A.4. The Ti II emission lines, cont.

λ_{calc}(Å)	Elem	log gf	E_{low}(cm^{-1})	conf.	E_{up}(cm^{-1})	conf.	R_c(obs)	R_c(calc)	Notes
6141.516	Ti II	−0.325	65460.010	(3F)4d f2F	81738.130	(3F)4f 4I	1.000	0.987	
6418.376	Ti II	+0.001	66794.010	(3F)4d 2P	82369.970	(3F)4f 2P	1.007	0.980	
6431.383	Ti II	−0.366	66521.010	(3F)4d 2P	82043.850	(3F)4f 4P	1.009	0.991	
6439.486	Ti II	−0.071	66794.010	(3F)4d 2P	82318.910	(3F)4f 2D	1.008	0.983	
6445.572	Ti II	−0.947	66794.010	(3F)4d 2P	82304.250	(3F)4f 4S	1.023	0.998	broad
6961.471	Ti II	+0.716	67822.490	(3F)4d e2G	82183.310	(3F)4f 2H	1.064	0.934	
6982.314	Ti II	+0.454	67606.640	(3F)4d e2G	81923.990	(3F)4f 2H	1.015	0.960	
7012.686	Ti II	+0.244	67822.490	(3F)4d e2G	82078.430	(3F)4f 4G	1.025	0.979	
7050.978	Ti II	+0.118	67822.490	(3F)4d e2G	82001.010	(3F)4f 2I	1.018	0.984	
7074.144	Ti II	+0.075	67606.040	(3F)4d e2G	81738.130	(3F)4f 4I	1.017	0.986	
7100.431	Ti II	−0.040	67606.040	(3F)4d e2G	81685.810	(3F)4f 2G	1.013	0.989	
7105.230	Ti II	−0.099	67606.040	(3F)4d e2G	81676.300	(3F)4f 4H	1.010	0.990	
7225.270	Ti II	+0.335	68482.410	(3F)4d 2D	82318.910	(3F)4f 2D	1.025	0.978	
7296.684	Ti II	−0.401	68364.390	(3F)4d 2D	82065.470	(3F)4f 2D	1.025	0.996	
7297.291	Ti II	+1.006	68584.280	(3F)4d e2H	82284.220	(3F)4f 2I	1.039	0.918	
7313.279	Ti II	+0.793	68331.020	(3F)4d e2H	82001.010	(3F)4f 2I	1.051	0.944	
7351.440	Ti II	+0.237	68331.020	(3F)4d e2H	82183.310	(3F)4f 2H	1.026	0.983	
7426.911	Ti II	−0.902	68482.410	(3F)4d 2D	81943.250	(3F)4f 2F	1.008	0.999	?
7443.684	Ti II	−0.580	68482.410	(3F)4d 2D	81912.920	(3F)4f 4F	1.005	0.997	?
7447.870	Ti II	+0.122	68331.020	(3F)4d e2H	81753.980	(3F)4f 4H	1.006	0.987	?
7574.057	Ti II	−0.703	68951.980	(3F)4d f4F	82151.310	(3F)4f 2F	1.012	0.998	
7653.044	Ti II	+0.606	69084.440	(3F)4d f4F	82147.540	(3F)4f 4F	1.016	0.969	
7679.192	Ti II	+0.661	69084.440	(3F)4d f4F	82103.060	(3F)4f 4G	1.013	0.965	
7681.729	Ti II	+0.194	68846.520	(3F)4d f4F	81860.840	(3F)4f 4G	1.012	0.987	
7706.784	Ti II	+0.346	68951.980	(3F)4d f4F	81923.990	(3F)4f 2H	1.020	0.982	
7713.367	Ti II	+0.273	68951.980	(3F)4d f4F	81912.920	(3F)4f 4F	1.011	0.985	
7716.915	Ti II	+0.429	68769.190	(3F)4d f4F	81724.170	(3F)4f 4G	1.010	0.978	
7733.343	Ti II	+0.035	68846.520	(3F)4d f4F	81773.980	(3F)4f 4F	1.013	0.991	
7786.450	Ti II	+0.251	68846.520	(3F)4d f4F	81685.810	(3F)4f 2G	1.011	0.986	
7805.972	Ti II	+0.128	71461.590	(3F)5p 4G	84268.770	(3F)5d 4G	1.006	0.991	?
7820.346	Ti II	+0.296	71586.060	(3F)5p 4G	84369.700	(3F)5d 4G	1.011	0.987	
7824.913	Ti II	+0.984	71945.900	(3F)5p 4G	84722.080	(3F)5d 4H	1.024	0.946	
7831.699	Ti II	+0.423	71747.460	(3F)5p 4G	84512.570	(3F)5d 4G	1.016	0.983	
7845.102	Ti II	+0.821	71747.460	(3F)5p 4G	84490.760	(3F)5d 4H	1.007	0.960	
7856.805	Ti II	+0.003	68951.980	(3F)4d f4F	81676.300	(3F)4f 4H	1.003	0.990	?
7869.297	Ti II	+0.616	71461.590	(3F)5p 4G	84165.710	(3F)5d 4H	1.000	0.973	?
7880.457	Ti II	+0.506	71945.900	(3F)5p 4G	84632.030	(3F)5d 4G	1.005	0.980	?
7994.391	Ti II	+0.566	72126.700	(3F)5p 4F	84632.030	(3F)5d 4G	1.017	0.979	
8838.415	Ti II	+0.517	71945.900	(3F)5p 4G	83257.040	(3F)6s 4F	1.016	0.973	?
8926.578	Ti II	+0.349	63445.880	(3F)5s e2F	74645.080	(3F)5p 2D	1.023	0.946	
9654.718	Ti II	+0.418	63445.880	(3F)5s e2F	73800.670	(2D)sp 2F	1.053	0.946	
9907.939	Ti II	−0.003	62180.160	(3F)5s e4F	72270.310	(3F)5p 4D	1.023	0.969	
9931.897	Ti II	+0.209	62272.160	(3F)5s e4F	72337.970	(3F)5p 4D	1.059	0.953	bad spectrum
9956.695	Ti II	+0.397	62410.780	(3F)5s e4F	72451.520	(3F)5p 4D	1.012	0.934	bad spectrum
9983.462	Ti II	+0.557	62595.030	(3F)5s e4F	72608.850	(3F)5p 4D	1.058	0.915	

[a] The symbol "*" indicates blended lines. The symbol " ?" indicates doubtful emissions

Table A.5. The Cr II emission lines. The line data are from Kurucz & Bell (1995).

λ_{calc}(Å)	Elem	log gf	E$_{low}$(cm^{-1})	conf	E$_{up}$(cm^{-1})	conf.	R$_c$(obs)	R$_c$(calc)	Notes[a]
6121.434	Cr II	−0.280	89277.950	(5D)4d e4P	105609.470	(5D)4f 6G	1.000	0.992	?
6128.189	Cr II	−0.492	89325.320	(5D)4d e4G	105638.840	(5D)4f 6F	1.007	0.995	
6158.621	Cr II	+0.718	89174.080	(5D)4d e4G	105406.990	(5D)4f 4H	0.990	0.928	
6161.031	Cr II	+0.573	89056.020	(5D)4d e4G	105282.580	(5D)4f 4H	1.002	0.945	
6172.927	Cr II	−0.239	89336.890	(5D)4d e4P	105532.180	(5D)4f 4D	1.012	0.991	
6179.226	Cr II	−0.055	89724.270	(5D)4d f4D	105903.050	(5D)4f 4F	1.007	0.987	
6181.354	Cr II	+0.189	89812.420	(5D)4d f4D	105985.630	(5D)4f 4F	1.017	0.978	
6182.340	Cr II	+0.452	89336.890	(5D)4d e4P	105507.520	(5D)4f 4D	1.023	0.960	
6186.315	Cr II	+0.336	89885.080	(5D)4d f4D	106045.320	(5D)4f 4G	1.009	0.971	
6193.551	Cr II	+0.012	89056.020	(5D)4d e4G	105197.380	(5D)4f 6H	1.000	0.984	
6209.250	Cr II	−0.169	89885.080	(5D)4d f4D	105985.630	(5D)4f 4F	1.009	0.990	
6213.078	Cr II	+0.037	89812.420	(5D)4d f4D	105903.050	(5D)4f 4F	1.008	0.985	
6213.538	Cr II	+0.143	89174.080	(5D)4d e4G	105263.520	(5D)4f 6H	1.000	0.979	
6231.676	Cr II	+0.061	89325.320	(5D)4d e4G	105367.930	(5D)4f 6H	1.000	0.983	
6237.002	Cr II	−0.104	89254.560	(5D)4d e4P	105283.470	(5D)4f 4P	1.003	0.988	
6285.601	Cr II	−0.229	89885.080	(5D)4d f4D	105790.060	(5D)4f 4F	1.028	0.992	
6299.534	Cr II	−0.679	89336.890	(5D)4d e4P	105206.690	(4F)sp p4D	1.015	1.000	
6301.413	Cr II	−0.162	89812.420	(5D)4d f4D	105677.490	(5D)4f 4G	1.009	0.990	
6309.669	Cr II	−0.013	89277.950	(5D)4d e4P	105122.260	(5D)4f 4P	1.013	0.986	
6311.509	Cr II	−0.190	89885.080	(5D)4d f4D	105724.770	(5D)4f 4G	1.008	0.991	
6324.198	Cr II	−0.121	89724.270	(5D)4d f4D	105532.180	(5D)4f 4D	1.015	0.990	
6369.654	Cr II	−0.692	89812.420	(5D)4d f4D	105507.520	(5D)4f 4D	1.008	0.997	
6399.280	Cr II	+0.004	89885.080	(5D)4d f4D	105507.520	(5D)4f 4D	1.004	0.987	
6501.575	Cr II	−0.310	90608.990	(5D)4d e4F	105985.630	(5D)4f 4F	1.011	0.994	
6526.302	Cr II	+0.173	89885.080	(5D)4d f4D	105203.460	(4F)sp r4F	1.003	0.982	
6536.680	Cr II	+0.026	90680.990	(5D)4d e4F	105903.050	(5D)4f 4F	1.016	0.988	
6551.373	Cr II	+0.229	90725.870	(5D)4d e4F	105985.630	(5D)4f 4F	1.025	0.982	
6579.572	Cr II	+0.215	90850.960	(5D)4d e4F	106045.320	(5D)4f 4G	1.019	0.983	
6585.241	Cr II	+0.829	90850.960	(5D)4d e4F	106032.240	(5D)4f 4G	1.030	0.939	
6592.341	Cr II	+0.217	90512.560	(5D)4d e4F	105677.490	(5D)4f 4G	1.021	0.982	
6613.776	Cr II	+0.485	90608.990	(5D)4d e4F	105724.770	(5D)4f 4G	1.007	0.968	
6636.427	Cr II	+0.573	90725.870	(5D)4d e4F	105790.060	(5D)4f 4F	1.029	0.963	
6656.120	Cr II	+0.066	90512.560	(5D)4d e4F	105532.180	(5D)4f 4D	1.005	0.987	
7211.765	Cr II	+0.656	93143.880	(5D)5p 6F	107006.290	(5D)5d 6G	1.000	0.963	
7226.064	Cr II	+0.791	93276.860	(5D)5p 6F	107111.840	(5D)5d 6G	1.011	0.953	
7242.963	Cr II	+0.904	93444.170	(5D)5p 6F	107246.870	(5D)5d 6G	1.000	0.943	
7394.889	Cr II	+0.451	94177.180	(5D)5p 6D	107696.310	(5D)5d 6D	1.000	0.980	
9448.293	Cr II	+0.179	84495.700	(5D)5s e4D	95076.720	(5D)5p 4D	1.048	0.956	
9951.294	Cr II	+0.126	84209.880	(5D)5s e4D	94256.070	(5D)5p 4F	1.042	0.971	
9952.493	Cr II	+0.318	84320.210	(5D)5s e4D	94365.190	(5D)5p 4F	1.024	0.957	
9970.727	Cr II	+0.477	84495.700	(5D)5s e4D	94522.310	(5D)5p 4F	1.048	0.943	
9974.826	Cr II	+0.535	84726.710	(5D)6s e4D	94749.200	(5D)5p 4F	1.024	0.938	

[a] The symbol " ?" indicates doubtful emissions

Table A.6. Line data and total hyperfine splitting in a sample of Mn II lines.

Mult.	λ^a(Å)	log gf	Ref.^{b}	χ_{low}(cm^{-1})	χ_{up}(cm^{-1})	hfs$_{\rm tot}$(Å)	Notes^c
– –	3159.302,hfs	−1.720	K,K88	62587.50	94230.90	0.077	no fit, TWC
– –	3330.778,hfs	−0.659	K,K88	37851.47	67865.85	0.031	
– –	3364.213	−1.956	K,K88	52383.72	82099.82	no data	hfs
– –	3366.028,hfs	−2.880	K,K88	43696.19	73396.26	0.045	no fit, TWC
– –	3366.121,hfs	−2.181	K,K88	43696.19	73395.44	0.052	no fit, TWC
– –	3418.232,hfs	−2.024	K,K88	44138.96	73385.46	0.031	
1	3438.974	−2.293	K,MFW	9472.97	38543.08	no data	hfs
3	3441.988,hfs	−0.272	K,MFW	14325.86	43370.51	0.011	
– –	3457.801,hfs	−2.338	K,K88	43395.38	72307.21	0.061	no fit, TWC
1	3460.030,hfs	−2.561	K,K88	9472.97	38543.08	0.026	
3	3460.316,hfs	−0.542	K,MFW	14593.82	43484.64	0.015	
– –	3461.458,hfs	−1.614	K,K88	44899.82	73781.11	0.044	
– –	3462.341,hfs	−2.099	K,K88	44521.52	73395.44	0.013	no fit
3	3474.040,hfs	−0.999	K,MFW	14593.82	43370.51	0.011	
3	3474.129,hfs	−1.089	K,MFW	14781.19	43557.14	0.018	
3	3482.905,hfs	−0.740	K,MFW	14781.19	43484.64	0.014	
3	3488.677,hfs	−0.864	K,MFW	14901.18	43557.14	0.018	
3	3495.833,hfs	−1.218	K,MFW	14959.84	43557.14	0.018	
3	3496.809,hfs	−1.687	K,MFW	14781.19	43370.51	0.009	
3	3497.526,hfs	−1.330	K,MFW	14901.18	43484.64	0.014	
– –	3509.939,hfs	−1.324	K,K88	43528.64	72011.02	0.096	
– –	3685.051,hfs	−1.299	K,K88	43528.64	70657.58	0.106	blend with Mn II 3685.042 Å
– –	3695.917,hfs	−1.966	K,K88	43696.19	70745.38	0.072	
– –	3763.730	−1.360	K,K88	41182.53	67744.37	no data	hfs
– –	3812.239	−1.897	K,K88	44521.52	70745.38	no data	hfs
– –	3844.161	−1.379	K,K88	44521.52	70527.62	no data	hfs
– –	3848.574	−3.333	K,K88	44521.52	70497.80	no data	hfs
– –	3897.604,hfs	−1.697	K,K88	43395.38	69044.90	0.078	no fit, TSC
– –	3917.318,hfs	−1.147	K,K88	55759.27	81279.71	0.046	
– –	3943.858,hfs	−2.464	K,K88	43696.19	69044.90	0.082	no fit, TWC
– –	3995.317,hfs	−2.441	K,K88	43395.38	68417.61	0.096	no fit, TSC
– –	4000.033,hfs	−1.212	K,K88	62587.50	87580.23	0.123	no fit, TSC
– –	4039.681,hfs	−3.357	K,K88	43537.18	68284.62	0.097	
– –	4136.902	−1.290	K,K88	49517.58	73683.44	no data	hfs
2	4174.318	−3.548	K,K88	14593.820	38543.08	0.001	
2	4205.375*	−3.376	K,K88	14593.820	38366.18	0.039	
7	4206.368*,hfs	−1.566	K,K88	43528.64	67295.43	0.129	
2	4207.234	−4.470	K,K88	14781.190	38543.08	0.002	no fit, TSC
– –	4237.861*	−2.959	K,K88	43311.30	66901.44	0.002	
2	4238.785*	−3.626	K,K88	14781.190	38366.18	0.038	
– –	4239.184*,hfs	−2.250	K,K88	43311.30	66894.09	0.050	
– –	4240.385*	−2.066	K,K88	49820.16	73396.26	0.071	
– –	4242.329*	−1.262	K,K88	49820.16	73385.46	0.057	blend with Cr II
– –	4242.920*	−2.992	K,K88	43339.42	66901.44	0.035	
7	4244.246*	−2.396	K,K88	43339.42	66894.09	0.038	
– –	4247.954*	−3.379	K,K88	43395.38	66929.52	0.087	TWC, large disagreement
– –	4251.727*	−1.058	K,K88	49882.15	73395.44	0.012	
– –	4252.961*	−1.138	K,K88	49889.86	73396.26	0.018	blend with Mn II
7	4253.018*	−2.403	K,K88	43395.38	66901.44	0.08	blend with Mn II
– –	4253.124*	−2.092	K,K88	49889.86	73395.44	0.018	blend with Mn II
7	4259.191*,hfs	−1.589	K,K88	43537.18	67009.16	0.094	
2	4260.462*	−4.246	K,K88	14901.180	38366.180	0.038	TSC
– –	4281.948*	−2.554	K,K88	43339.42	66686.70	0.029	blend with Mn II
– –	4282.490,hfs	−1.679	K,K88	44521.52	67865.85	0.052	
6	4283.766*,hfs	−2.204	K,K88	43339.42	66676.78	0.028	
6	4284.429	−2.265	K,K88	43311.30	66645.07	0.025	

Table A.6. Line data and total hyperfine splitting in a sample of Mn II lines, cont.

Mult.	λ^a (Å)	log gf	Ref.^{b}	χ_{low}(cm^{-1})	χ_{up}(cm^{-1})	hfs$_{tot}$(Å)	Notes^c
−−	4288.067*	−1.890	K,K88	33906.57	77220.56	0.013	
−−	4289.595*	−3.306	K,K88	43339.42	66645.07	0.027	TWC
6	4292.233*,hfs	−2.226	K,K88	43395.38	66686.70	0.077	no fit, TWC
6	4300.254*,hfs	−2.880	K,K88	43395.38	66643.31	0.079	no fit, TWC
−−	4302.957*	−6.136	K,K88	43696.19	66929.52	0.093	observed, not predicted
−−	4308.153*	−1.723	K,K88	43696.19	66901.44	0.092	
−−	4317.720*	−1.917	K,K88	55759.27	78913.17	0.032	
6	4325.047*,hfs	−2.299	K,K88	43528.64	66643.31	0.119	
6	4326.643*,hfs	−1.254	K,K88	43537.18	66643.31	0.091	
−−	4336.959*	−2.551	K,K88	43850.42	66901.44	0.020	
−−	4338.345*	−2.090	K,K88	43850.42	66894.09	0.039	
−−	4382.579*	−1.977	K,K88	44745.46	67766.76	0.041	
6	4343.983*,hfs	−1.095	K,K88	43528.64	66542.53	0.118	
6	4345.593*	−2.164	K,K88	43537.18	66542.53	0.090	
−−	4346.406*	−1.544	K,K88	52718.80	75719.93	0.004	
−−	4348.396*,hfs	−1.500	K,K88	43696.19	66686.70	0.082	
−−	4356.628*	−2.026	K,K88	43696.19	66643.31	0.084	
−−	4363.254*	−1.909	K,K88	44899.82	67812.05	0.041	
−−	4365.220*	−1.350	K,K88	53017.16	75919.09	0.006	
−−	4377.744*,hfs	−2.144	K,K88	43850.42	66686.70	0.017	
−−	4379.644*,hfs	−1.850	K,K88	43850.42	66676.78	0.018	
−−	4385.738*	−3.029	K,K88	43850.42	66645.07	0.016	
−−	4403.513*	−1.804	K,K88	53017.16	75719.93	0.004	
−−	4434.062*	−1.514	K,K88	53017.16	75563.49	0.000	blend with Mg II
−−	4441.996*	−2.355	K,K88	44138.96	66645.07	0.026	
−−	4478.635*	−0.950	K,K88	53597.13	75919.09	0.007	
−−	4518.953*	−1.329	K,K88	53597.13	75719.93	0.007	
5	4727.841,hfs	−2.017	K,K88	43311.30	64456.69	0.015	no fit
5	4730.395,hfs	−2.147	K,K88	43339.42	64473.39	0.047	
5	4738.290,hfs	−2.244	K,K88	43395.38	64494.14	0.115	no fit
5	4755.727,hfs	−1.242	K,K88	43528.64	64550.04	0.176	large disagreement
5	4764.728,hfs	−1.351	K,K88	43537.18	64518.87	0.136	large disagreement
−−	5102.517	−1.934	K,K88	48317.85	67910.56	no data	hfs
−−	5177.648	−1.772	K,K88	48435.96	67744.37	no data	hfs
−−	5294.315	−0.037	K,K88	79540.87	98423.80	no data	hfs
−−	5295.384	+0.360	K,K88	79544.68	98423.80	no data	hfs
−−	5295.412	+0.360	K,K88	79544.68	98423.70	no data	hfs
−−	6008.190	−1.271	K,K88	83255.79	99895.13	no data	hfs
−−	6009.205	−1.050	K,K88	83255.79	99892.32	no data	hfs
−−	6009.858	−1.096	K,K88	83255.79	99890.51	no data	hfs
−−	6411.004,hfs	−1.487	K,K88	66452.53	82136.40	0.105	
−−	7083.538*	−3.089	K,K88	53698.70	67812.05	0.103	
−−	7098.194*	−3.083	K,K88	53781.71	67865.85	0.076	
−−	7106.329*	−2.171	K,K88	53698.70	67766.76	0.108	
−−	7110.354*	−1.923	K,K88	53805.80	67865.85	0.077	
−−	7125.441*	−2.059	K,K88	53781.71	67812.05	0.077	
−−	7137.694*	−2.976	K,K88	53805.80	67812.05	0.073	
−−	7148.506*	−3.016	K,K88	53781.71	67766.76	0.105	blend with telluric lines
−−	7323.762*	−3.210	K,K88	54846.24	68496.61	0.055	
−−	7330.577*,hfs	−2.713	K,K88	29919.43	43557.14	0.359	
−−	7347.813*,hfs	−3.814	K,K88	29951.42	43557.14	0.253	
−−	7353.549*,hfs	−2.726	K,K88	29889.52	43484.64	0.385	
−−	7369.763*,hfs	−3.174	K,K88	29919.43	43484.64	0.350	
−−	7373.426*	−2.806	K,K88	54938.19	68496.61	0.068	
−−	7387.184*,hfs	−2.553	K,K88	29951.42	43484.64	0.242	
−−	7415.803*,hfs	−2.202	K,K88	29889.52	43370.51	0.373	

Table A.6. Line data and total hyperfine splitting in a sample of Mn II lines, cont.

Mult.	λ^a (Å)	log gf	Ref.^{b}	χ_{low}(cm^{-1})	χ_{up}(cm^{-1})	hfs$_{tot}$(Å)	Notes^c
– –	7416.637*	−3.703	K,K88	54938.19	68417.61	0.061	
– –	7432.294*,hfs	−2.498	K,K88	29919.43	43370.51	0.337	
– –	7471.581*	−2.877	K,K88	55166.31	68496.61	0.094	
– –	7490.309*	−3.019	K,K88	62572.20	75919.09	0.196	
– –	7490.752*	−2.779	K,K88	65567.07	78913.17	0.081	
– –	7498.931*	−2.282	K,K88	62587.50	75919.09	0.416	not observed
– –	7515.955*	−2.917	K,K88	55116.31	68417.61	0.087	blend with Fe II
– –	7942.111*	−2.456	K,K88	55696.99	68284.62	0.148	
– –	9407.015,hfs	−2.554	K,K88	32857.19	43484.64	0.109	TWC
– –	9408.696,hfs	−2.951	K,K88	32859.09	43484.64	0.109	TWC
– –	9446.846,hfs	−2.389	K,K88	32787.87	43370.51	0.079	TWC

[a] (hfs) the hyperfine components are included in the adopted line lists; (*) the wavelength is from Holt et al. (1999)

[b] "K" before another log gf source means that the log gf is from Kurucz files available at http://kurucz.harvard.edu/linelists/gf100
K88: Kurucz 1988; MFW: Martin et al. 1988

[c] (TWC) the computed profile is weaker than the observed one ; (TSC) the computed profile is stronger than the observed one; (hfs) observed hyperfine broadening

Table A.7. The Ga II lines analysed. When the two isotopes Ga^{69} and Ga^{71} are considered separately, the oscillator strengths are log $gf(Ga^{69})$=−0.222 and log $gf(Ga^{71})$=−0.398.

Isot.	λ(Å)	log gf_{iso}	log gf_{hfs}	log gf_{comp}
	4251.149	log gf_{tot}=+0.35		
69+71	4251.112	0.0	−2.049	−1.699
69+71	4251.130	0.0	−0.766	−0.416
69+71	4251.167	0.0	−0.086	+0.264
	4254.075	log gf_{tot}=−0.23		
69+71	4254.047	0.0	−0.338	−0.568
69+71	4250.070	0.0	−0.599	−0.829
69+71	4254.092	0.0	−0.741	−0.971
69+71	4254.111	0.0	−0.970	−1.200
	4255.722	log gf_{tot}=+0.634		
69+71	4255.622	0.0	−1.385	−0.751
69+71	4255.642	0.0	−1.406	−0.772
69+71	4255.657	0.0	−1.534	−0.900
69+71	4255.672	0.0	−1.148	−0.514
69+71	4255.688	0.0	−1.746	−1.112
69+71	4255.716	0.0	−0.453	+0.181
69+71	4255.742	0.0	−1.200	−0.566
69+71	4255.774	0.0	−0.597	+0.037
69+71	4255.791	0.0	−0.876	−0.242
	4255.937	log gf_{tot}=−0.32		
69+71	4255.818	0.0	−1.631	−1.951
69+71	4255.839	0.0	−1.915	−2.235
69+71	4255.857	0.0	−1.330	−1.650
69+71	4255.904	0.0	−0.677	−0.997
69+71	4255.924	0.0	−0.839	−1.159
69+71	4255.949	0.0	−1.251	−1.571
69+71	4255.971	0.0	−1.100	−1.420
69+71	4255.994	0.0	−0.718	−1.038
69+71	4256.013	0.0	−0.899	−1.219
	4261.4780	log gf_{tot}=−1.10		
69+71	4261.432	0.0	−0.757	−1.857
69+71	4261.448	0.0	−0.699	−1.799
69+71	4261.477	0.0	−1.000	−2.100
69+71	4261.509	0.0	−0.280	−1.380
	4262.014	log gf_{tot}=+0.98		
69+71	4262.010	0.0	−0.016	+0.964
69+71	4262.051	0.0	−1.525	−0.545
69+71	4262.067	0.0	−2.228	−1.248
	4263.1361	log gf_{tot}=−0.50		
69+71	4262.983	0.0	−1.204	−1.704
69+71	4263.018	0.0	−1.169	−1.669
69+71	4263.050	0.0	−1.204	−1.704
69+71	4263.070	0.0	−1.137	−1.637
69+71	4263.097	0.0	−1.505	−2.005
69+71	4263.113	0.0	−1.584	−2.084
69+71	4263.144	0.0	−0.593	−1.093
69+71	4263.176	0.0	−1.505	−2.005
69+71	4263.239	0.0	−0.621	−1.121
69+71	4263.266	0.0	−0.821	−1.321
	5338.240	log gf_{tot}=+0.43		
71	5338.137	−0.398	−0.778	−0.746
69	5338.159	−0.222	−0.783	−0.575
71	5338.199	−0.398	−0.477	−0.445
69	5338.208	−0.222	−0.475	−0.267
69	5338.289	−0.222	−0.301	−0.093
71	5338.302	−0.398	−0.301	−0.269

Isot.	λ(Å)	log gf_{iso}	log gf_{hfs}	log gf_{comp}
	5360.4022	log gf_{tot}=+0.42		
71	5360.314	−0.398	−1.079	−1.057
69	5360.334	−0.222	−1.079	−0.881
71	5360.335	−0.398	−1.079	−1.057
69	5360.350	−0.222	−1.079	−0.881
71	5360.357	−0.398	−0.678	−0.656
69	5360.368	−0.222	−0.678	−0.480
71	5360.391	−0.398	−0.972	−0.950
71	5360.394	−0.222	−0.972	−0.774
69	5360.411	−0.222	−1.778	−1.580
71	5360.412	−0.398	−1.778	−1.756
69	5360.432	−0.222	−0.398	−0.200
71	5360.438	−0.398	−0.398	−0.376
69	5360.469	−0.222	−1.046	−0.848
71	5360.486	−0.398	−1.044	−1.022
69	5360.496	−0.222	−2.000	−1.802
71	5360.521	−0.398	−2.000	−1.978
	5363.5854	log gf_{tot}=+0.06		
71	5363.353	−0.398	−1.556	−1.894
69	5363.402	−0.222	−1.556	−1.718
71	5363.416	−0.398	−0.857	−1.195
71	5363.430	−0.398	−0.857	−1.195
69	5363.451	−0.222	−0.857	−1.019
69	5363.463	−0.222	−0.857	−1.019
71	5363.493	−0.398	−1.352	−1.690
69	5363.512	−0.222	−1.352	−1.514
69	5363.594	−0.222	−0.824	−0.986
71	5363.597	−0.398	−0.824	−1.162
69	5363.613	−0.222	−0.824	−0.986
71	5363.621	−0.398	−0.824	−1.162
69	5363.695	−0.222	−0.456	−0.618
71	5363.725	−0.398	−0.456	−0.794
	5416.3179	log gf_{tot}=+0.64		
71	5416.287	−0.398	−0.796	−0.554
71	5416.292	−0.398	−1.000	−0.758
69	5416.295	−0.222	−0.796	−0.378
71	5416.296	−0.398	−0.611	−0.369
69	5416.299	−0.222	−1.000	−0.582
69	5416.302	−0.222	−0.611	−0.193
71	5416.320	−0.398	−0.447	−0.205
69	5416.321	−0.222	−0.447	−0.029
69	5416.350	−0.222	−1.398	−0.980
71	5416.356	−0.398	−1.398	−1.156
69	5416.378	−0.222	−1.282	−0.864
71	5416.393	−0.398	−1.282	−1.040
69	5416.419	−0.222	−1.389	−0.971
69	5416.433	−0.222	−2.544	−2.126
71	5416.444	−0.398	−1.389	−1.147
71	5416.462	−0.398	−2.544	−2.302
69	5416.495	−0.222	−2.690	−2.272
71	5416.541	−0.398	−2.690	−2.448

Table A.7. The Ga II lines analysed, cont.

Isot.	λ(Å)	log $gf_{\rm iso}$	log $gf_{\rm hfs}$	log $gf_{\rm comp}$
	5421.2746	log $gf_{\rm tot}$=−0.05		
71	5421.122	−0.398	−1.301	−1.749
71	5421.143	−0.398	−1.301	−1.749
71	5421.152	−0.398	−1.155	−1.603
69	5421.156	−0.222	−1.301	−1.573
69	5421.172	−0.222	−1.301	−1.573
69	5421.179	−0.222	−1.155	−1.427
71	5421.186	−0.398	−1.097	−1.545
69	5421.206	−0.222	−1.097	−1.369
71	5421.207	−0.398	−1.301	−1.749
71	5421.211	−0.398	−1.243	−1.691
69	5421.223	−0.222	−1.301	−1.573
69	5421.226	−0.222	−1.243	−1.515
71	5421.259	−0.398	−0.762	−1.210
69	5421.264	−0.222	−0.762	−1.034
69	5421.291	−0.222	−1.155	−1.427
71	5421.294	−0.398	−1.155	−1.603
69	5421.344	−0.222	−0.465	−0.737
71	5421.361	−0.398	−0.465	−0.913
69	5421.382	−0.222	−1.243	−1.515
71	5421.409	−0.398	−1.243	−1.691
	6419.2391	log $gf_{\rm tot}$=+0.57		
71	6418.970	−0.398	−0.859	−0.687
71	6418.991	−0.398	−0.824	−0.652
69	6419.030	−0.222	−0.857	−0.509
69	6419.047	−0.222	−0.824	−0.476
71	6419.080	−0.398	−1.556	−1.384
69	6419.117	−0.222	−1.556	−1.208
71	6419.175	−0.398	−1.352	−1.180
69	6419.191	−0.222	−1.352	−1.004
69	6419.278	−0.222	−0.857	−0.509
71	6419.284	−0.398	−0.857	−0.685
69	6419.315	−0.222	−0.456	−0.108
71	6419.332	−0.398	−0.456	−0.284
69	6419.459	−0.222	−0.824	−0.476
71	6419.516	−0.398	−0.824	−0.652

Isot.	λ(Å)	log $gf_{\rm iso}$	log $gf_{\rm hfs}$	log $gf_{\rm comp}$
	6334.0688	log $gf_{\rm tot}$=+1.00		
71	6333.911	−0.398	−1.079	−0.477
69	6333.948	−0.222	−1.079	−0.301
71	6333.964	−0.398	−0.678	+0.076
69	6333.989	−0.222	−0.678	+0.100
71	6333.998	−0.398	−1.079	−0.477
69	6334.017	−0.222	−1.079	−0.301
69	6334.089	−0.222	−0.398	+0.380
71	6334.091	−0.398	−0.398	+0.204
69	6334.104	−0.222	−0.972	−0.194
71	6334.110	−0.398	−0.972	−0.370
69	6334.173	−0.222	−1.778	−1.000
71	6334.198	−0.398	−1.778	−1.176
69	6334.250	−0.222	−1.046	−0.268
71	6334.295	−0.398	−1.046	−0.444
69	6334.365	−0.222	−2.000	−1.222
71	6334.442	−0.398	−2.000	−1.398
	6455.9231	log $gf_{\rm tot}$=−0.08		
71	6455.578	−0.398	−0.778	−1.256
69	6455.653	−0.222	−0.778	−1.080
71	6455.784	−0.398	−0.477	−0.955
69	6455.816	−0.222	−0.477	−0.779
69	6456.087	−0.222	−0.301	−0.603
71	6456.123	−0.398	−0.301	−0.779

Table A.8. Isotopic and hyperfine structure of Ba II 4554 Å.

Isot.	λ(Å)	log $gf_{\rm iso}$	log $gf_{\rm hfs}$	log $gf_{\rm comp}$
	4554.029	log $gf_{\rm tot}$ = +0.163		
137	4553.995	−0.950	−0.806	−1.573
137	4553.997	−0.950	−0.806	−1.573
137	4553.998	−0.950	−1.204	−1.991
135	4553.999	−1.181	−0.806	−1.824
135	4554.001	−1.181	−0.806	−1.824
135	4554.001	−1.181	−1.204	−2.222
138	4554.029	−0.144	0.000	+0.019
134	4554.029	−1.617	0.000	−1.454
136	4554.029	−1.105	0.000	−0.942
135	4554.046	−1.181	−0.359	−1.377
135	4554.049	−1.181	−0.806	−1.824
137	4554.049	−0.950	−0.359	−1.146
135	4554.050	−1.181	−1.505	−2.523
137	4554.051	−0.950	−0.806	−1.573
137	4554.052	−0.950	−1.505	−2.291

Table A.9. Isotopic and hyperfine structure of H I at 4358 Å and Hg II at 3984 and 6149 Å

Isot.	λ(Å)	log $gf_{\rm iso}$	log $gf_{\rm hfs}$	log $gf_{\rm comp}$
Hg I	*4358.3Å*	log $gf_{\rm tot}$=−0.323		
199a	4358.175	−1.301	−0.959	−2.583
201a	4358.228	−1.301	−0.832	−2.456
201b	4358.341	−1.301	−0.862	−2.486
201c	4358.288	−1.301	−1.552	−3.176
199b	4358.314	−1.301	−0.259	−1.883
201d	4358.316	−1.301	−1.352	−2.976
204	4358.320	−1.523	0.000	−1.846
202	4358.326	−0.432	0.000	−0.755
200	4358.332	−0.456	0.000	−0.779
198	4358.337	−0.886	0.000	−1.209
196	4358.341	−50.000	0.000	−50.323
201e	4358.352	−1.301	−0.462	−2.086
201f	4358.362	−1.301	−0.862	−2.486
199c	4358.379	−1.301	−0.649	−2.273
201g	4358.442	−1.301	−0.832	−2.456
199d	4358.520	−1.301	−0.959	−2.583
Hg II	*3983.89Å*	log $gf_{\rm tot}$=−1.520		
196	3983.771	0.000	−50.000	−51.520
198	3983.839	−0.886	0.000	−2.406
199a	3983.844	−1.301	−0.373	−3.194
199b	3983.853	−1.301	−0.240	−3.061
200	3983.912	−0.456	0.000	−1.976
201a	3983.932	−1.301	−0.438	−3.259
201b	3983.941	−1.301	−0.201	−3.022
202	3983.993	−0.432	0.000	−1.952
204	3984.072	−1.523	0.000	−3.043
Hg II	*6149.47Å*	log $gf_{\rm tot}$=+0.150		
199a	6149.419	−1.301	−0.436	−1.587
201a	6149.451	−1.301	−0.239	−1.390
204	6149.461	−1.523	0.000	−1.373
202	6149.469	−0.432	0.000	−0.282
200	6149.477	−0.456	0.000	−0.306
198	6149.483	−0.886	0.000	−0.736
199b	6149.504	−1.301	−0.198	−1.349
201b	6149.513	−1.301	−0.373	−1.524

Table A.10. Unidentified absorption lines.

λ_{calc}(Å)	Notes[a]
4735.55	Mn I 4635.542 ?
4753.20	Mn I 4753.226, Mn II 4753.179
4783.15	
4927.12	
4942.10	bl Fe II 4942.177
4977.53	
4991.60	
5031.28	
5036.30	
5037.87	
5038.30	
5038.87	Cr I 5038.87 ?
5040.12	
5043.65	
5044.55	
5057.00	Hf II 5057.03 ?
5058.15	Hf II 5058.15 ?
5073.45	
5084.30	
5090.60	
5091.60	Mn II 5091.608, strong
5098.28	strong
5101.83	
5104.75	
5105.85	Mn II 5105.889, As II ? strong
5121.87	
5122.05	
5126.00	
5126.20	
5126.83	
5127.20	
5127.33	
5128.48	
5128.60	
5130.00	
5130.17	
5130.63	
5131.70	
5132.00	
5134.06	
5134.16	
5135.27	
5136.15	
5136.30	
5138.60	
5139.07	
5139.25	Fe I 5139.251
5140.20	
5145.50	
5148.55	
5149.25	
5152.70	
5152.98	
5153.78	
5156.45	
5157.50	
5158.07	
5163.00	
5163.58	
5164.92	
5165.70	
5166.20	
5167.125	
5167.7	
5167.82	
5170.125	
5171.30	
5176.725	
5177.40	
5179.15	
5179.55	
5181.65	
5186.10	
5190.00	
5190.45	
5192.75	
5193.725	
5194.40	
5195.10	
5195.225	
5195.95	
5210.55	
5215.20	
5221.05	
5222.175	
5225.25	
5225.35	
5226.05	
5228.625	
5234.30	
5236.00	
5236.35	
5236.45	
5237.675	
5238.475	
5239.35	
5240.325	
5240.575	
5241.20	
5244.975	
5245.075	
5246.55	
5247.70	
5248.35	
5257.35	
5258.675	
5260.100	
5261.20	
5261.60	
5270.30	
5272.05	
5274.20	
5277.80	
5281.35	
5282.225	
5282.50	
5283.075	
5284.00	
5284.575	
5288.825	
5290.10	
5300.125	
5304.65	
5305.15	
5305.40	
5306.35	
5308.80	
5311.075	
5321.825	
5327.15	
5327.75	
5329.35	
5330.55	Br II
5331.23	As II ?
5332.975	
5336.20	
5340.25	
5341.7	
5342.05	
5348.35	
5350.70	
5354.40	
5355.90	
5357.1	
5359.75	
5383.5	
5390.60	
5410.35	
5451.75	
5482.7	
5497.7	As II ?
5505.75	
5506.35	
5513.425	
5515.20	
5516.00	
5518.075	
5518.20	
5518.525	
5521.875	
5533.1	
5533.4	
5536.575	
5537.075	
5537.45	
5558.075	As II ?
5620.00	
5651.3	As II ?
5660.5	
5706.35	Si II 5706.37 ?
5734.3	
5753.85	

[a] The symbol "?" indicates possible identifications

Table A.11. Unidentified emission lines

λ_{obs}(Å)	R_c(obs)	Notes[a]
6000.15	1.018	
6037.93	1.020	
6146.07	1.013	
6177.50	1.027	
6255.37	1.018	
6312.25	1.021	
6344.80	1.019	
6447.10	1.018	
6534.15	1.025	
6618.50	1.016	
6745.32	1.013	Cr II 6745.239 ?
6814.40	1.031	
6845.15	1.037	
6849.80	1.010	
7453.67	1.013	
7662.90	1.042	
8493.12	1.022	
8676.70	1.020	
8706.30	1.007	
8721.55	1.013	
8732.65	1.016	
8761.60	1.022	Mn II 8761.644 ?
9032.95	1.035	
9036.12	1.086	
9208.45	1.041	Mn II 9208.604 ?
9242.65	1.033	Mn II 9242.744 ?
9394.00	1.055	
9497.465	1.021	Fe II ?
9573.25	1.051	

[a] The symbol " ?" indicates possible identifications